

~~40896~~

FACILITY FORM 602

N64-29227
(ACCESSION NUMBER)

84
(PAGES)

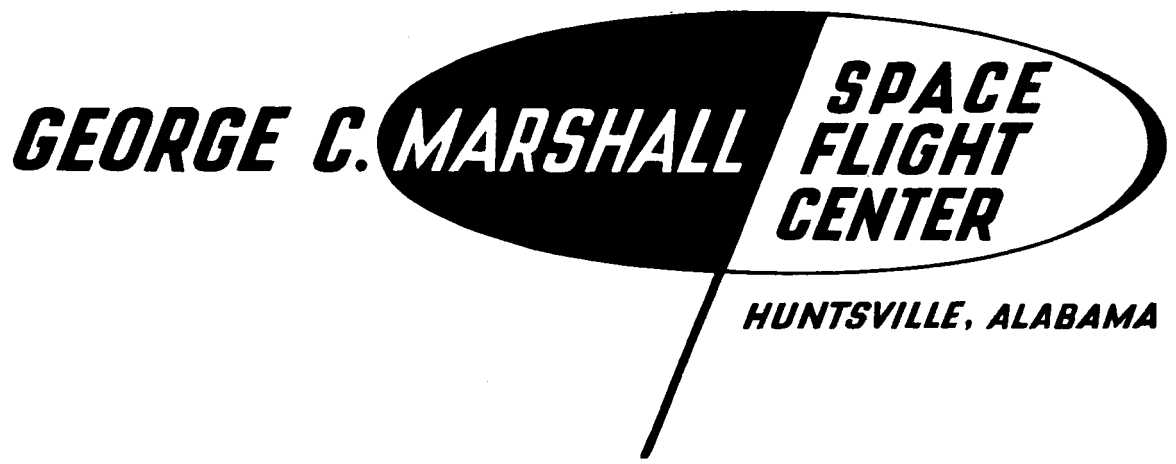
TMX-51919
(NASA CR OR TMX OR AD NUMBER)

(THRU) _____

(CODE) **27**

(CATEGORY) _____

MTP-P&VE-P-62-10
November 8, 1962



ENGINE-INTEGRATED SECONDARY INJECTION SIDE-FORCE
GENERATION FOR THE HYDROGEN-FUELED ROCKET ENGINE

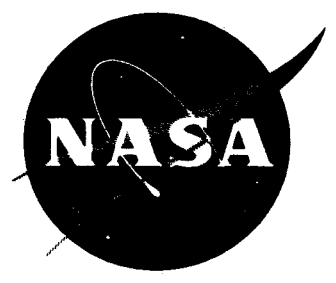
By

William J. D. Escher
and
Donald D. Thompson

OTS PRICE

XEROX \$ 8.10 ph

MICROFILM \$ _____



FOR INTERNAL USE ONLY

GEORGE C. MARSHALL SPACE FLIGHT CENTER

MTP-P&VE-P-62-10

ENGINE-INTEGRATED SECONDARY INJECTION SIDE-FORCE
GENERATION FOR THE HYDROGEN-FUELED ROCKET ENGINE

By William J. D. Escher and Donald D. Thompson

ABSTRACT

A promising alternative to gimbaling of large, massive hydrogen-fueled rocket engines is the concept of side-force generation through gaseous secondary injection.

This report presents an analysis of the mechanism of gaseous secondary injection, and a review of the existing background of work in this area--with emphasis on the current lack of engineering level effort, especially on hydrogen-fueled engines.

To acquire the much-needed hydrogen-oriented information, Marshall Space Flight Center recently contracted a program; sufficient information to define an optimal subsystem should be available by the Spring of 1963. The scope of that contracted effort is described herein.

In the meanwhile it is recommended that a complementary hardware-level engineering effort be initiated to contribute to the definition of a practicable secondary injection subsystem for the hydrogen-fueled engine. Feasible configurations of a gaseous secondary injection subsystem are suggested, together with an example comparison of the gimbaling and secondary injection concepts.

Author

GEORGE C. MARSHALL SPACE FLIGHT CENTER

MTP-P&VE-P-62-10

ENGINE-INTEGRATED SECONDARY INJECTION SIDE-FORCE
GENERATION FOR THE HYDROGEN-FUELED ROCKET ENGINE

By William J. D. Escher and Donald D. Thompson

PROPULSION AND MECHANICS BRANCH
PROPULSION AND VEHICLE ENGINEERING DIVISION

LIST OF ILLUSTRATIONS

Figure	Title	Page
1a	Representation of Vehicle with Engine Thrust Acting Through Vehicle Center-of-Mass	3
1b	Representation of Vehicle with Engine Thrust Not Acting Through Vehicle Center-of-Mass	3
1c	Resolution of Thrust Vector Into Axial and Side Components	3
1d	Generation of Controlled Vehicle Turning Moment Through Engine Gimbaling	4
1e	Generation of Controlled Vehicle Turning Moment Through Secondary Injection	5
1f	Generation of Controlled Vehicle Turning Moment Through Differential Thrust-Level Operation	5
2	Injection Configurations Tested by Pratt and Whitney; Injectants: Hydrogen and Nitrogen, Ambient Temperature	7
3	Effect of Port Location on Lateral Force for Sonic Circular Injection Port	9
4	Effect of Primary Nozzle Area Ratio on Lateral Force for Sonic Circular Injection Port	10
5	Schematic Diagram of Generalized Flow Model Employed in Analysis of Secondary Injection Thrust Vector Control	12
6	Performance of Improved Secondary Injection Configuration	15
7	Variation of Amplification Factor with Angle of Upstream Injection	16

TABLE OF CONTENTS

	Page
SUMMARY	1
INTRODUCTION	3
BACKGROUND AND CURRENT SUPPORTING WORK	5
THE GASEOUS SECONDARY INJECTION FLOW	
PHENOMENON	8
General	8
Mechanism of Secondary Injection	11
Increasing the Efficiency of the	
Basic Configuration	13
Nozzle Wall Pressure Field	
with Secondary Injection	17
Analytical Expression for	
Side Force	19
Comparison of Experimental and	
Theoretical Data	21
Correlation of Hot-Flow and Cold-	
Flow Data	25
ENGINE INTEGRATED SECONDARY INJECTION	
SUBSYSTEM	27
VEHICLE CONSIDERATIONS	38
SOME COMPARATIVE POINTS: SECONDARY INJECTION	
VIS A VIS GIMBALING	42
1. Equipment Complexity	42
2. Point of Side-Force Application	47
3. Response in Side-Force Generation	49
4. Overall Performance	50
APPENDIX I.	57
APPENDIX II.	58
APPENDIX III.	63
REFERENCES	74

LIST OF ILLUSTRATIONS (CONTINUED)

Figure	Title	Page
8	Pressure Distribution on Nozzle Wall During Vectoring.	18
9	Variation of Lateral Amplification Factor with Injection Angle.	22
10	Variation of Lateral Amplification Factor with Primary Nozzle Area Ratio.	22
11	Variation of Lateral Amplification Factor with Injection Mach Number.	24
12	Some Alternative Approaches for Effecting Secondary Injection.	31
12a	Turbine Exhaust Utilization	31
12b	Alternative Turbine Exhaust Utilization Scheme.	32
12c	Combustion Gas with Hydrogen Dilution.	33
12d	Auxiliary Combustion Devices.	33
12e	Thrust Chamber Hydrogen Dump Cooling	36
12f	Very-High Performance Using High-Temperature Hydrogen.	36
13	Comparison of Possible Powerplant Arrangements with Gimbale and Secondary Injection Versions of the M-1 Engine.	39
14	Gimbale and Secondary Injection Versions of Model M-1 Stage.	41
15	Engine Specific Impulse Versus Effective Gimbal Angle.	42

LIST OF ILLUSTRATIONS (CONCLUDED)

Figure	Title	Page
16	Review of Component Inventory: Secondary Injection Vis a Vis Gimbaling.	44
16a	Typical Mechanization for Gimbaling.	44
16b	Secondary Injection with Single-Acting Valves	45
16c	Secondary Injection with Double-Acting Valves	46
16d	Secondary Injection with Single Multi-Port Valve.	46
17	Comparison of Point of Side Force Application Between Gimbaled and Secondary Injection Cases.	47
18	Comparative Side Force Response	50
19	Relative Payload Performance Aspects of Gimbaling and Secondary Injection Versus Thrust Vector Deflection Operating Point.	52
20	Lateral Amplification Factor Versus Secondary Flow-Weight Ratio for the M-1 Using Turbine Exhaust Secondary Injection.	67
21	Axial Specific Impulse Contribution of Secondary Injectant Versus Secondary Flow-Weight Ratio .	71

DEFINITION OF SYMBOLS

SYMBOL	DEFINITION
a	Local Acoustic Velocity
AR or ϵ	Area ratio of primary nozzle
C	Efficiency parameter
I_{SP}	Specific Impulse
Mom	Moment
f	Separation parameter
f_2D	Two-dimensional separation parameter
F_1	Axial Thrust
F_2	Total lateral force
g	Acceleration of Gravity: 32.17 Ft/Sec ²
K_1	Uncorrected lateral amplification factor
K_2	Lateral amplification factor
M	Mach number
m	Molecular Weight
P	Pressure
T	(Total) Temperature
V	Velocity
\dot{W}	Weight Flow
α	Angle of upstream injection

DEFINITION OF SYMBOLS (CONCLUDED)

SYMBOL	DEFINITION
λ	Stage Propellant Mass Fraction
ϕ_i	Induced side force parameter
ϕ_2	Momentum side force parameter
θ	Flow Angle at Exit
δ	Gimbal Angle
ρ	Density
γ	Ratio of Specific Heats

Subscripts

1	Primary Flow
2	Secondary flow
a	Ambient Condition
e	Exit Condition
S	Side Direction
TE	Turbine Exhaust
AX	Axial Direction
2-D	Two Dimensional
T	Total or Stagnation Conditions

Superscript

* Applies to Flow at Sonic Conditions

GEORGE C. MARSHALL SPACE FLIGHT CENTER

MTP-P&VE-P-62-10

ENGINE-INTEGRATED SECONDARY INJECTION SIDE-FORCE
GENERATION FOR THE HYDROGEN-FUELED ROCKET ENGINE

By William J. D. Escher and Donald D. Thompson

SUMMARY

This report is restricted to secondary injection side-force generation as it applies to hydrogen-fueled rocket engines; the reason is two-fold:

- a. NASA interest in propulsion for launch vehicles has focused increasingly on engines using hydrogen as a propellant.
- b. Hydrogen--as a component of the secondary injectant--produces very high side-force performance. That is, it has a potential for achieving a very high side-specific-impulse. Consequently, no auxiliary fluid is needed.

The concept of engine side-force generation (gaseous secondary injection in hydrogen-fueled engines) is reviewed briefly as background for this report. Much analytical and experimental research has been conducted in secondary injection; however, coherent supporting work applicable to the use of hydrogen as an injectant--either alone or in conjunction with combustion products--is insubstantial. To provide the needed analytical results and a substantiating experimental program, MSFC recently contracted with the Research Laboratory of the United Aircraft Corporation (NAS8-5070) for a nine-month study effort focused on hydrogen secondary injection. The scope of this work is outlined in Appendix I. Final results should be available in the Spring of 1963.

Autho

The gaseous secondary injection mechanism is discussed and an analytical model is presented in this report. Emphasis is put on the attractiveness of hydrogen as a major constituent of the secondary injectant. Hydrogen performance is quite high and it is available from the engine itself; so, there is no need to consider the traditional "third fluid" (freon, hydrazine, etc.). The secondary injection process is viewed as an engine-integrated subsystem and its desirable qualities are outlined. Such equipment must be thought of and treated always as a vital part of the engine fluid-flow circuit; therefore, the design, development, qualification, and field usage aspects must be **examined and** controlled as strictly as those of other major engine subsystems.

The primary advantages of secondary injection in large hydrogen-fueled vehicles are: (1) a fixed engine instead of a gimbaled one, and (2) accompanying this, the opportunity to use a higher nozzle expansion area ratio within a given diametral envelope. Since no gimbaling structure is needed, large concentrated dynamic loads at the gimbal block and actuator tie-points are avoided, permitting a gross shortening of the powerplant compartment and a significant weight reduction in its structural components. A basic powerplant rearrangement is possible and may be advantageous, such as clustering of the pumping units closer to the propellant tankage. The higher area ratio yields an increased powerplant specific impulse. Some of these advantages are demonstrated in this report with a simplified performance comparison among several versions of a hypothetical, large upper-stage vehicle in the Nova class.

It is felt that the majority of the requirements for hydrogen-oriented background information to establish optimal injection configuration and to evaluate nozzle scale effects will be satisfied by contracted work now underway. Therefore, we now recommend immediate initiation of an engine hardware-level engineering effort to:

- (1) establish a recommended subsystem approach to the configuration
- (2) highlight additional areas in which more background work is required, and
- (3) determine, in depth, the overall vehicular ramifications of secondary injection side-force generation.

INTRODUCTION

The rocket engine, fundamentally, is a force-producing device. After a rocket engine has been properly attached singly or in a multiple installation to a suitable space vehicle structure, its force does useful work in producing a path acceleration. FIG 1a illustrates this basic situation.



FIGURE 1a

If the engine force is directed through any point other than the instantaneous center of mass of the vehicle, then--in addition to path acceleration--an angular acceleration of the vehicle about its center of mass results (FIG 1b). The resulting rotation of the vehicle moves the line-of-force away from the desired orientation relative to the line of motion. Efficiency-wise--and for other reasons--this situation cannot normally be tolerated.

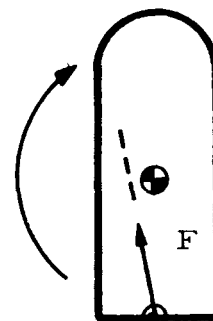


FIGURE 1b

The conditions depicted in FIG 1b can be shown in another way: the engine force (still viewed quite generally) can be separated vectorially into an axial force and a side-force as shown in FIG 1c. The axial force, F_{AX} , is defined as that component directed through the center of mass of the vehicle: the force component that accelerates the vehicle along the intended path. The side-force, F_s , is the angular acceleration component that turns the vehicle about its center of mass--if unopposed by a countering moment.

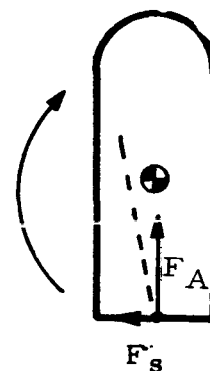


FIGURE 1c

Under the normal circumstances of rocket thrust-chamber positioning, alignment allowances and vehicle center of mass location uncertainties, an engine side-force will be present. Unless opposed by another force, say that generated by an aerodynamic control surface, the engine-caused side-force will disturb orientation of the vehicle. But if the engine side-force can be controlled in direction and magnitude, misalignment disturbance can be "self-cancelled" and disturbances from without such as those due to aerodynamic forces can be corrected.

Put more simply: the axial force component propels the vehicle in the direction of its extended centerline; the side-force component rotates the vehicle in some direction oblique to its centerline (providing a stabilizing and steering function). Our objective is to find or devise some way to generate and control a side-force component.

At the present time, for liquid propellant rocket engines the generally accepted method of developing engine side-forces is gimbaling (FIG 1d). In gimbaling, the thrust chamber, and often the entire engine, concentrates its total thrust at a pivotable structural connection usually called a gimbal block. The thrust chamber is thus deflectable about the gimbal by means of actuators (normally two) for pitch and yaw side-force generation. The gimbaling approach is quite successful, to the extent of being now almost universally accepted. It has distinct and decisive advantages over earlier side-force systems; for example, the jet vane, which it has by now largely supplanted. But, with the introduction of new, larger vehicles, some marked disadvantages of gimbaling have become increasingly apparent. Among these disadvantages are: (1) highly concentrated dynamic and static loads (gimbal block and actuator attach points), (2) requirement for flexible propellant lines, (3) high-powered actuation system, and (4) inability to maximize nozzle expansion area ratio in available vehicle envelope due to required gimbaling clearances.

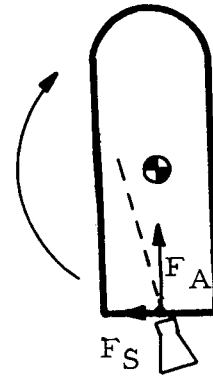


FIGURE 1d

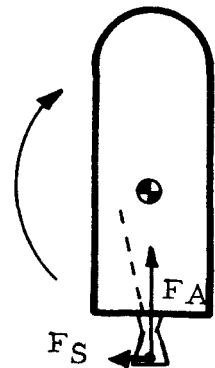
Large, massive hydrogen-fueled engines as presently designed (M-1*, Nerva), require proportionally massive gimbaling means. Very high, dynamic, concentrated actuation loads are involved. In turn, this leads to substantial increases in powerplant and stage weight in addition to that required for the basic propulsion means. Hence, alternative methods of producing controlled engine side-forces are much in demand.

Two of the more promising alternatives under consideration employ fixed rather than movable engines. Both are fluid-control (as opposed to mechanical) types:

*The M-1 engine is currently undergoing a program reorientation which may result in a non-gimbaled design as an alternative approach.

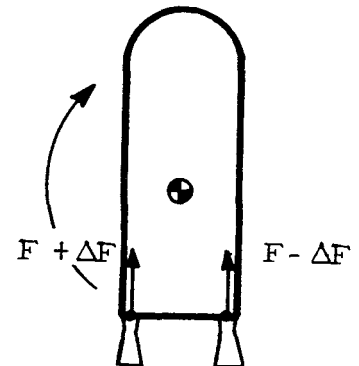
1. Line-of-thrust deflection induced via secondary fluid injection in the primary nozzle flow (applicable to propulsion systems having any number of expansion nozzles: FIG 1e).

FIGURE 1e



2. Differential thrust-level operation via selected apportionment of main propellant flow (normally applicable only to propulsion systems having three or more combustors and/or expansion nozzles: FIG 1f).

FIGURE 1f



Although the end-effect on the vehicle is identical, the mechanism involved in these two methods is significantly different. Vehicle side-forces result from variation in the direction of the thrust-vectors in the first case, and magnitude of the thrust-vectors, in the second case. This report deals only with the first of these two systems approaches: secondary injection.

BACKGROUND AND CURRENT SUPPORTING WORK

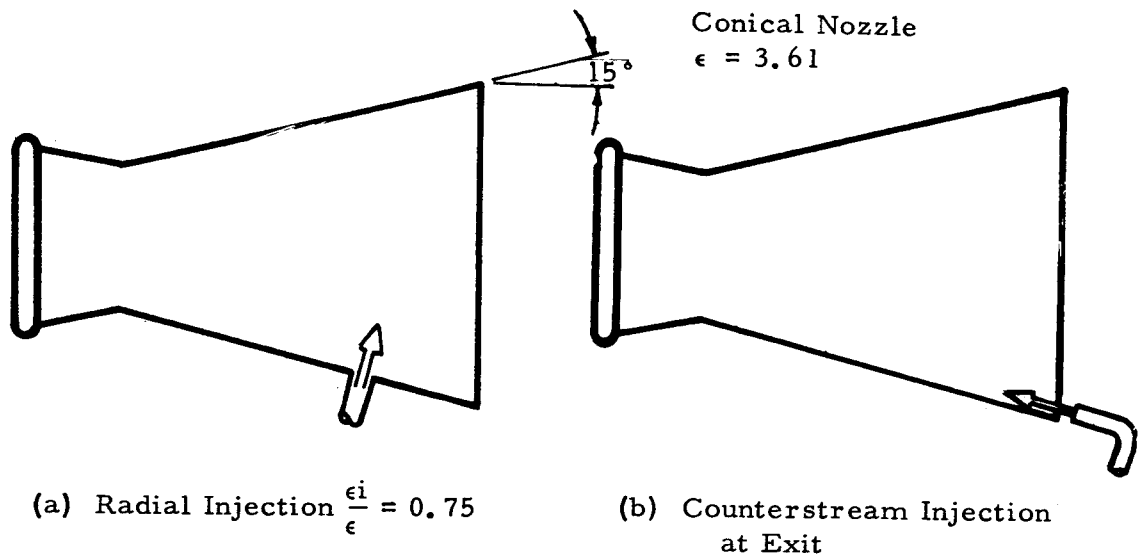
The concept of injecting a secondary fluid into rocket nozzles to generate side-forces for vehicle control is not new. It appears that the first serious consideration of this approach occurred around 1950 at the United Aircraft Corporation Research Laboratories. A patent for secondary fluid side-force generation was filed in 1950 (granted in 1960, No. 2,943,821) by A. E. Wetherbee, Jr. of UAC.

Interest and research activity in secondary injection for both liquid, and solid-propulsion systems have increased substantially in the last few years. Practically every rocket engine manufacturer has

performed some experiments and conducted analytical programs in secondary injection. In terms of sheer magnitude, the recent programs of United Technology Corporation, Aerojet-General, and the Lockheed Propulsion Company have been impressive. Here, secondary injection tests on large solid-propellant rockets (approaching one-half million pounds thrust) have been performed with both reactive and non-reactive liquid injection. So far as we know, secondary injection in liquid rockets has been limited to much lower thrust levels (60K-lb and less). There is a reason why the solid propellant industry has "taken the lead" in developing the technology of secondary injection. Since there is no direct equivalent of the rather effective method of generating side forces by thrust-chamber gimbaling, in the solid engine (swivel-nozzles such as found on the Minuteman missile notwithstanding) the solid propellant industry was stirred to develop an effective alternative. Secondary injection is today a favored method.

With the F-1 and J-2 liquid propellant engine programs now deep into their development phase, and with the M-1 engine program beginning, some of the salient disadvantages of gimbaling very large liquid engines have become particularly noticeable (note the discussion of this point in the Introduction, page 4). Quite naturally, serious interest in reviewing alternative schemes for feasibility has resulted. Side-force generation through secondary injection is receiving a considerable amount of this attention.

Erickson and Bell of Thiokol recently completed a most comprehensive survey of reported work in secondary injection (Ref. 1). This work--sponsored by the Air Force Systems Command--is oriented toward side-force generation in the solid-propellant rocket, but much of the discussion is applicable to liquid engines as well. In this report only one reference was cited in which hydrogen was employed as a secondary injectant. This work was performed by Chamay and Sederquist of Pratt and Whitney (Ref. 2). The primary nozzle flow in these experiments was developed with the UDMH- N_2O_4 propellant combination over a wide range of O/F values (1.9 - 5.2) with the hydrogen injectant at ambient temperature. Ambient nitrogen was also injected. Two injection configurations were used as shown in FIG 2. Hydrogen far exceeded nitrogen in performance as had been expected (molecular weight advantage discussed on page 26). Of the two injection configurations, the counter-stream injection port at the nozzle exit was the higher--considerably higher--performer.



MTP-P&VE-P-62-10

FIGURE 2. INJECTION CONFIGURATIONS TESTED BY PRATT AND WHITNEY;
INJECTANTS: HYDROGEN AND NITROGEN, AMBIENT TEMP. (REF 2)

The only other known work with hydrogen injection is the current test activity at Rocketdyne: hydrogen-oxygen combustion products from a small gas-generator injected into a RP-LOX 1K-lb vernier-type thrust chamber. This work is not yet complete, hence, performance data are not available at this time; however, initial results indicate high side-force performance by hydrogen.

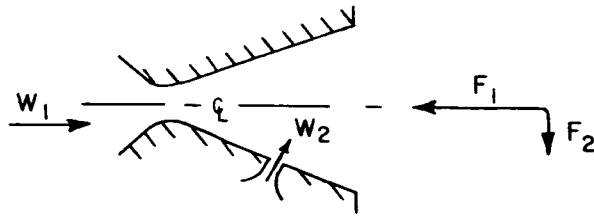
The scarcity of hydrogen-oriented work in secondary injection stimulated MSFC, under the auspices of the NASA Office of Advanced Research and Technology, to establish appropriate contracted work in this area with the Research Laboratory of the United Aircraft Corporation. For general information, the work statement for this contract (NAS8-5070) is included in this report as Appendix I. The final report on this effort should be published in the Spring of 1963.

THE GASEOUS SECONDARY INJECTION FLOW PHENOMENON

GENERAL

As mentioned earlier, the use of secondary fluid injection to obtain side-forces in rocket-powered vehicles was originally conceived at the United Aircraft Research Laboratories about 1950. The idea was investigated and proved feasible in the work reported in reference 3 which was published in 1952. This work, limited to nozzles having low area-ratios, showed that the lateral force produced is significantly greater than the theoretical value for a system utilizing a separate convergent-divergent secondary nozzle at the same station with its axis perpendicular to the axis of the primary nozzle. More extensive studies applicable to rocket nozzles having larger area ratios were subsequently conducted at the Research Laboratories and are reported in reference 4.

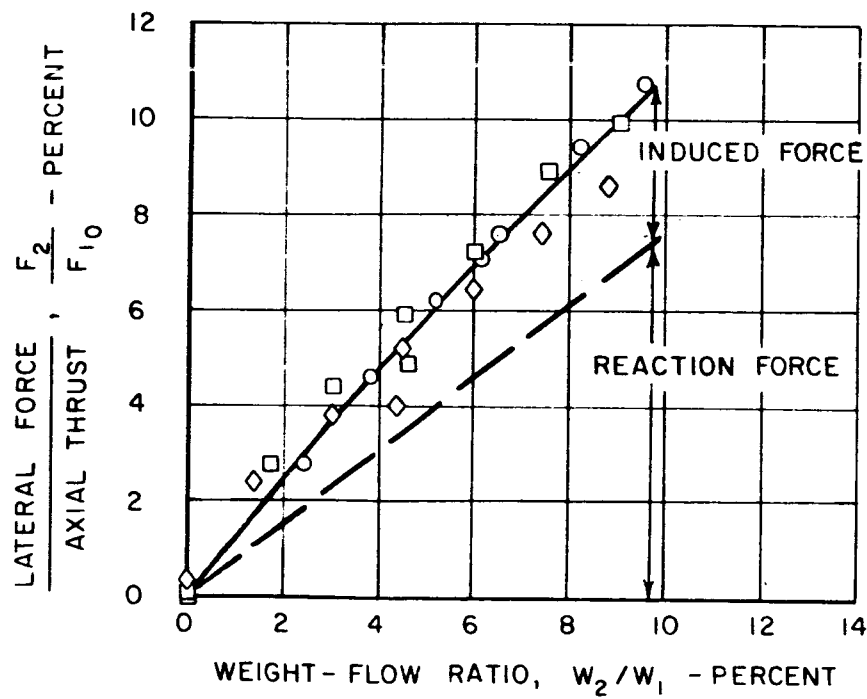
The results showed that the lateral force produced by secondary injection through a circular orifice perpendicular to the surface of a conical nozzle varies almost linearly with secondary flowrate and is independent of injection port location, nozzle area-ratio, and nozzle pressure ratio for a wide range of these variables. Typical results are shown in FIG 3 and 4.



CONICAL PRIMARY NOZZLE
AREA RATIO = 12:1
15-DEG HALF ANGLE

SONIC SECONDARY INJECTION
PERPENDICULAR TO WALL
THROUGH CIRCULAR ORIFICE

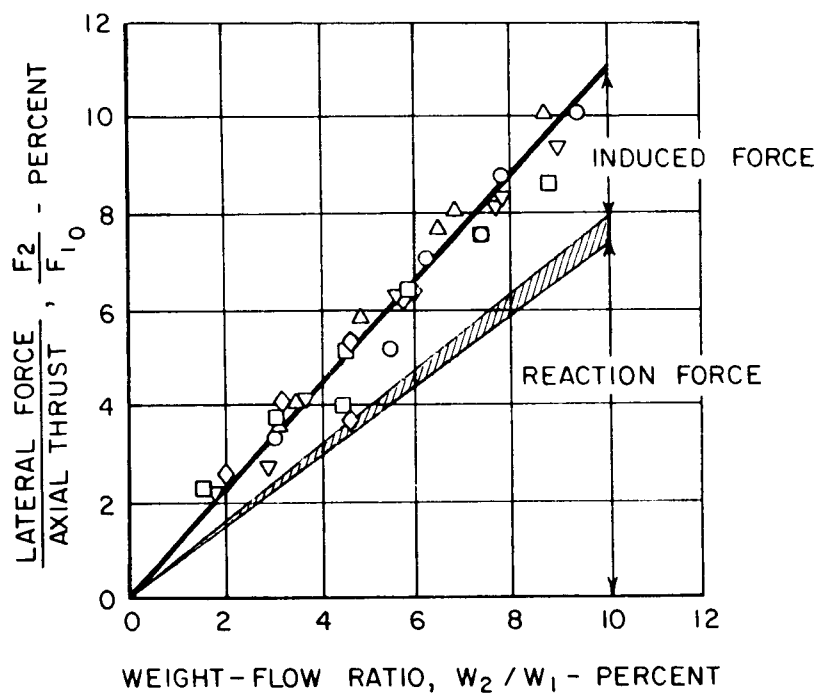
SYMBOL	AREA RATIO AT PORT STATION
○	6.0
□	8.0
◇	10.1



MTP-P&VE-P-62-10

FIGURE 3. EFFECT OF PORT LOCATION ON LATERAL FORCE
FOR SONIC CIRCULAR INJECTION PORT

SYMBOL	NOZZLE AREA RATIO	AREA RATIO AT PORT STATION
○	8.0	6.0
□	12.1	10.1
◇	15.5	13.5
△	20.0	18.0
▽	25.0	23.0



MTP-P&VE-P-62-10

FIGURE 4. EFFECT OF PRIMARY NOZZLE AREA RATIO ON LATERAL FORCE FOR SONIC CIRCULAR INJECTION PORT

Because of the three-dimensional nature of flow and the complexity of the shock wave phenomena, the problem of side-force generation by secondary injection does not lend itself readily to analysis. Nevertheless, a few attempts toward theoretical solution of the problem have been made using simplifying assumptions. However, to our present knowledge, there exists only one theoretical analysis which covers the phenomena adequately and which has shown good correlation with experimental results. This analysis (Appendix II) is based on that developed by the United Aircraft Corporation Research Laboratories. It is adopted for the presentation which follows in this section*.

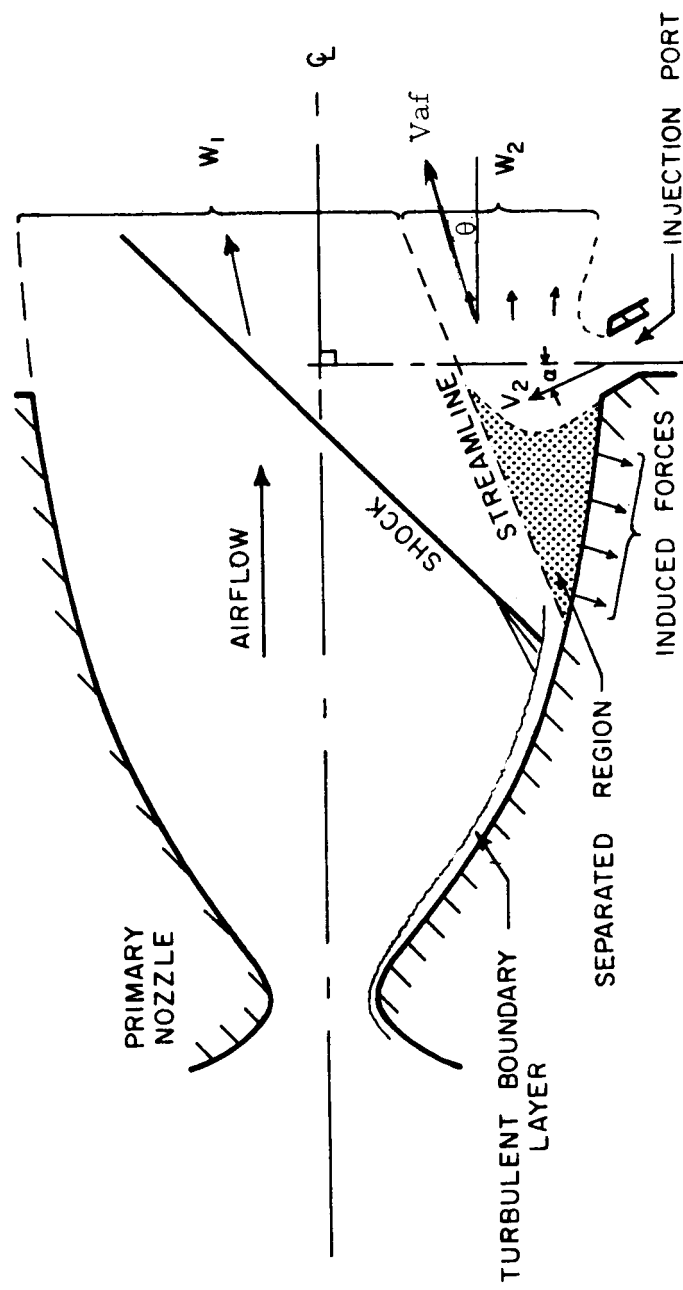
MECHANISM OF SECONDARY INJECTION

Before discussing the analyses, a description of the flow interaction phenomena is appropriate. Several investigators, making use of pressure distribution measurements, force balance systems, and visualization techniques (Schlieren, etc.) have presented various qualitative pictures of the flow phenomena, see references 5, 6, and 7.

The flow model to be used for the analyses here is presented in FIG 5. The step-by-step action involved in the formation of side-force by non-reacting gas injection (normally the case in the hydrogen-fueled rocket) is as follows:

1. The supersonic jet issuing from the injection nozzle acts as an obstruction to the supersonic flow of the main stream.
2. A detached, oblique, conical shock is formed in front of the jet.
3. Some of the compressed primary gas in the high pressure region behind the shock leaks down to the subsonic boundary layer reverses its direction, and flows forward (upstream) causing the boundary layer in front of the jet to separate from the wall.
4. The separated boundary layer now assumes the role of the primary obstruction to the main stream flow and forces the generation of a series of compression waves which, although not individually as

*FIG 3 through 11 are taken directly from reference 8,



MTP-P&VE-P-62-10

FIGURE 5. SCHEMATIC DIAGRAM OF GENERALIZED FLOW MODEL EMPLOYED IN ANALYSIS OF SECONDARY INJECTION THRUST VECTOR CONTROL

strong as the original primary shock, exhibit the same total effect on the primary flow.

5. The high pressure flow which separated the boundary layer next turns and expands outward and in a downstream direction, mixing with the incoming separated boundary layer.

6. The side-force due to the interaction of the two streams is produced by the high pressure acting on the area behind the jet, and separated boundary layer-induced shocks.

Investigations of the induced pressure field produced by injection from a circular port into a conical nozzle showed that there is a large increase in the wall pressure force immediately upstream of the port, but that there is a region of negative pressure (less than the value with secondary injection) downstream of the port. Also, the region of high pressure falls off rather rapidly around the circumference of the port.

INCREASING THE EFFICIENCY OF THE BASIC CONFIGURATION

The above findings indicate that the performance of a secondary injection system might be improved by increasing the aspect ratio; i. e., elongating the port, to minimize the circumferential pressure fall-off. Further, performance should be markedly increased by locating the injection port at the nozzle exit thus eliminating the negative pressure region from the nozzle.

Further, if it is assumed that the induced force is proportional to the change in momentum required to turn the secondary flow in a downstream direction, then directing the secondary flow upstream (which requires a larger change in momentum to turn the flow downstream) should produce a larger lateral force for a given amount of secondary flow.

In summary, these three actions should increase the efficiency of secondary injection:

1. Minimize circumferential pressure fall-off by employing elliptical ports (or approximating these with a greater number of smaller circular ports in a row).

2. Eliminate the negative pressure region by locating the injection port at the exit of the nozzle.

3. Utilize up-stream injection.

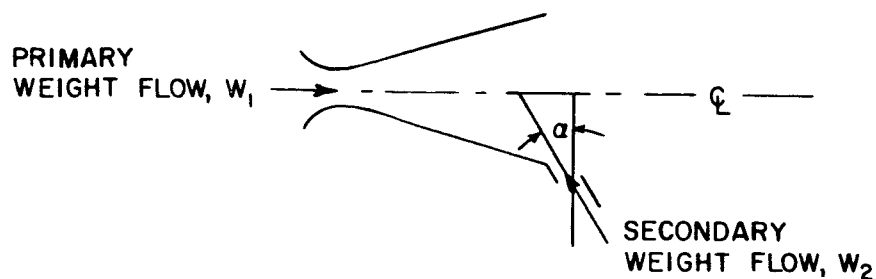
These three features were incorporated in an improved secondary injection system tested by the United Aircraft Corporation (Ref. 6). The injection geometry consisted of a circumferential slot at the nozzle exit. The performance of this configuration is compared with that of a perpendicular circular port in FIG 6. The improved configuration produced approximately 50 percent greater lateral force for an equal amount of secondary flow even though the axial force contribution of the secondary flow was reduced by the upstream injection.

Besides the improved performance obtained from this configuration, the exit location for the injection nozzle may be desirable from a nozzle fabrication standpoint because it does not require the primary nozzle structure to be altered to provide for secondary injection through the thrust-chamber wall.

Tests employing a slot at the nozzle exit were conducted to determine the optimum angle of injection. The results are presented in FIG 7 in terms of the lateral amplification factor, K_2 , defined by

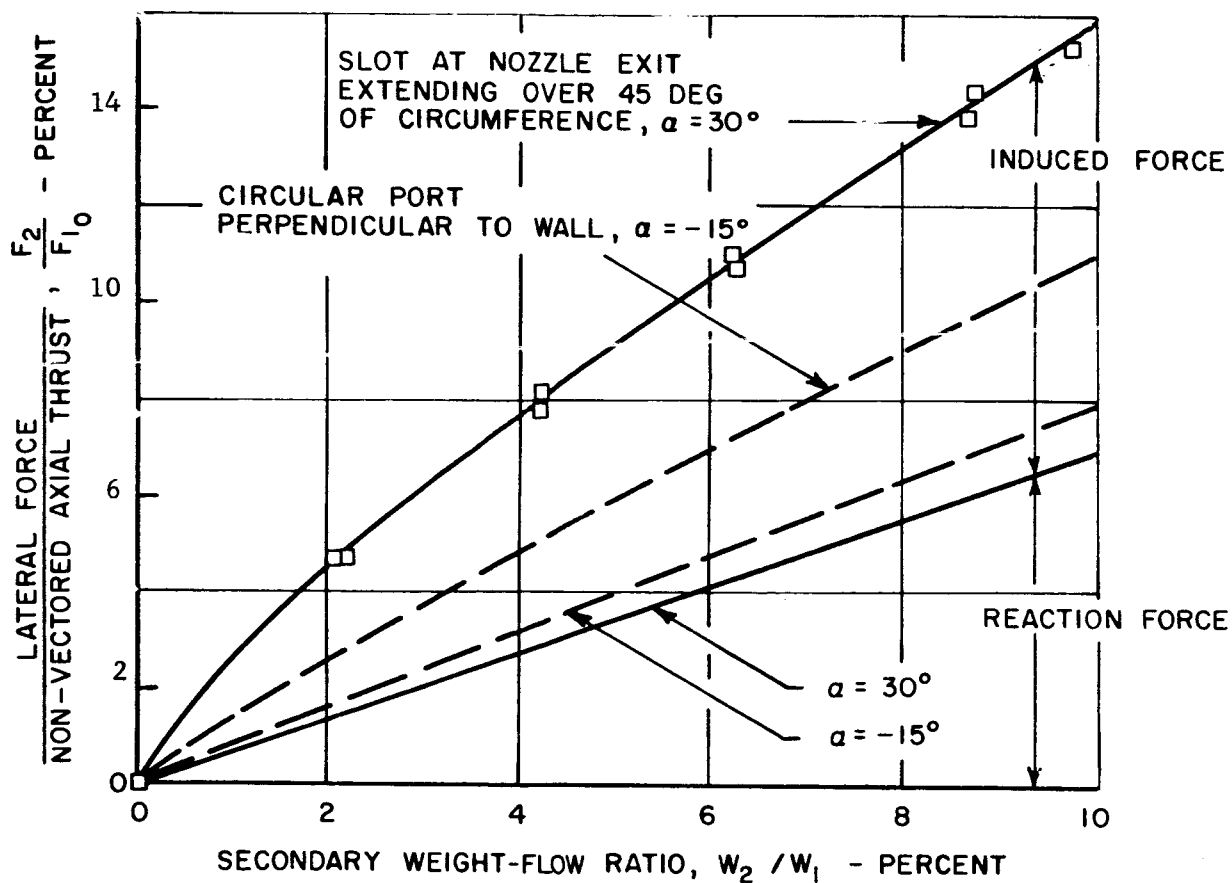
$$\frac{F_2}{F_1} = K_2 \times \frac{\dot{W}_2}{\dot{W}_1} \quad (1)$$

A system employing a separate secondary nozzle which produces the same specific impulse as the primary nozzle and is directed perpendicularly outward from the primary nozzle would have K_2 1.0. K_2 is greater than unity when the secondary injection system produces a specific impulse in the lateral direction which is higher than the axial specific impulse of the primary nozzle. For the data shown in FIG 7, K_2 increased from 1.15 for injection perpendicular to the wall to 1.8 for the optimal angle of injection which is between 30 and 45 degrees upstream. Included in FIG 7 are data from a



CONICAL NOZZLE
15-DEG HALF ANGLE
AREA RATIO = 12:1

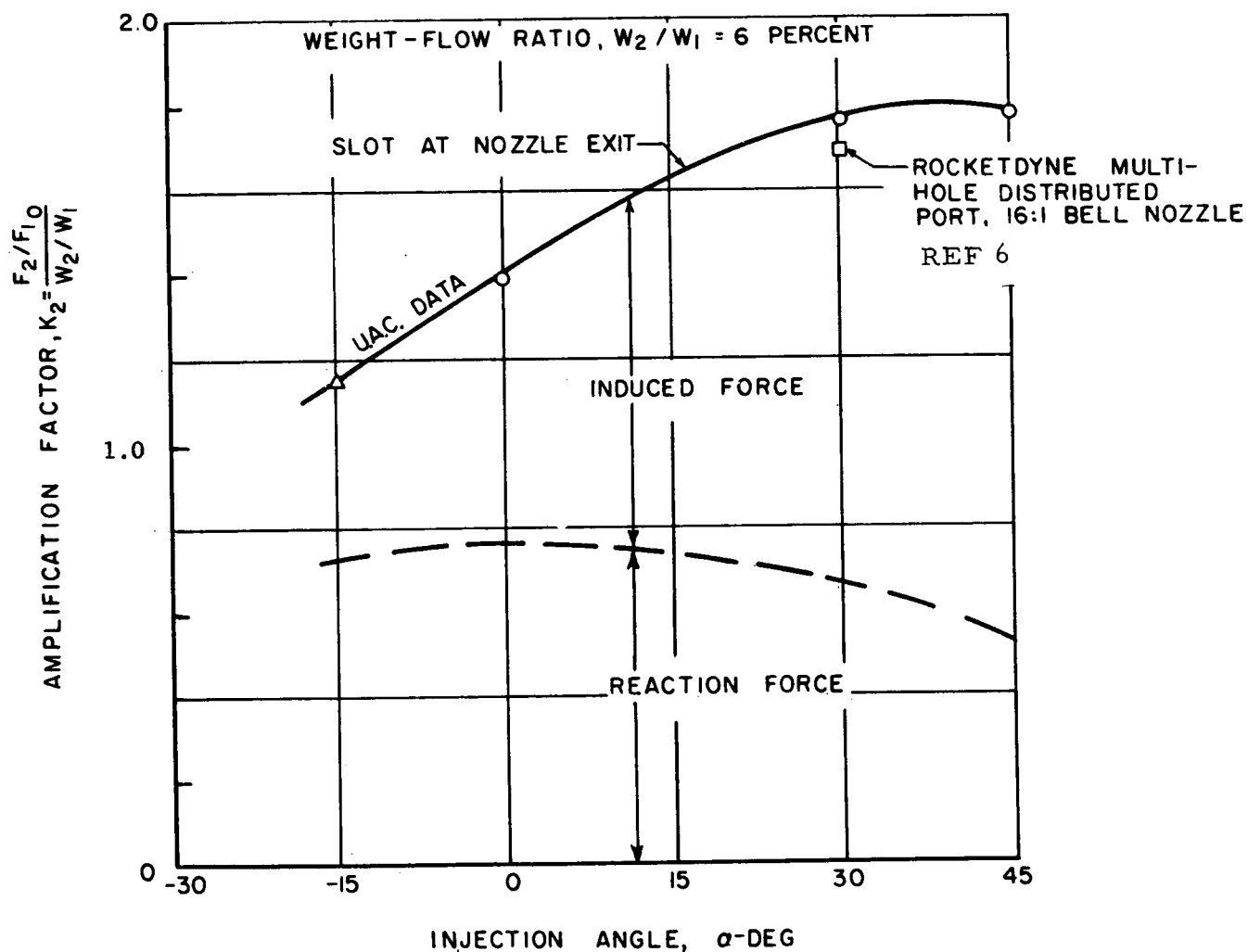
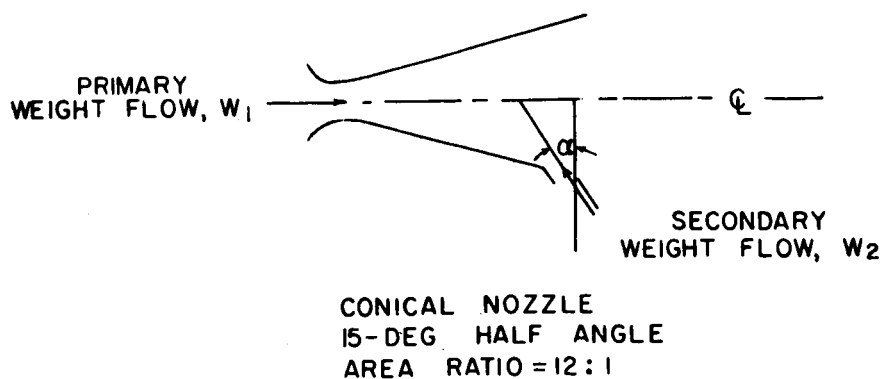
$$P_{T_1} / P_{AMB} = 180$$



MTP-P&VE-P-62-10

FIGURE 6. PERFORMANCE OF IMPROVED SECONDARY INJECTION CONFIGURATION

VARIATION OF AMPLIFICATION FACTOR WITH ANGLE OF UPSTREAM INJECTION



MTP-P&VE-P-62-10

FIGURE 7. VARIATION OF AMPLIFICATION FACTOR
WITH ANGLE OF UPSTREAM INJECTION

multihole port (distributed circumferentially at the nozzle exit) obtained from reference 6.

NOZZLE-WALL PRESSURE FIELD WITH SECONDARY INJECTION

Investigations have been made to determine the nature of the induced pressure field generated by secondary injection. In the case cited a conical nozzle was used with injection of a relatively large secondary weight flow upstream at an angle of 45 degrees through a slot at the nozzle exit. Detailed static pressure distributions were measured. A pressure contour map of the static pressure distribution is shown in FIG 8. In this figure the lower half of the primary nozzle is "unrolled" to show the nature of the pressure field. The location of the shock is several injection port widths upstream of the injection port and the pressure field extends to the sides of the nozzle.

Note that the effectiveness of the edges of an induced pressure field in producing a lateral force diminishes to zero as the circumferential angle goes to ± 90 degrees. This occurs because the pressure forces at these edges have no component in the desired lateral direction. For smaller secondary injection flow rates, the interaction field is more localized near the region of the injection port and thus results in a more effective utilization of the induced pressure forces. The greater circumferential spreading of the induced pressure field for the larger weight flows is one of the reasons why the effectiveness of secondary injection diminishes as the secondary weight flow is increased.

As shown in FIG 8, the static pressure ratio across the front of the induced shock is approximately 2.4. This value is consistent with the peak pressure ratio obtained from more general separation studies of the flow over a mechanical step as reported in reference 7. So, it appears that boundary layer separation criteria can be applied in analyzing the induced pressure field generated by secondary injection.

The work presented in reference 8 provides a good theoretical analysis which correlates quite well with experimental performance of thrust-vector control by secondary injection through a circumferential slot at the nozzle exit. The method of analysis relates the

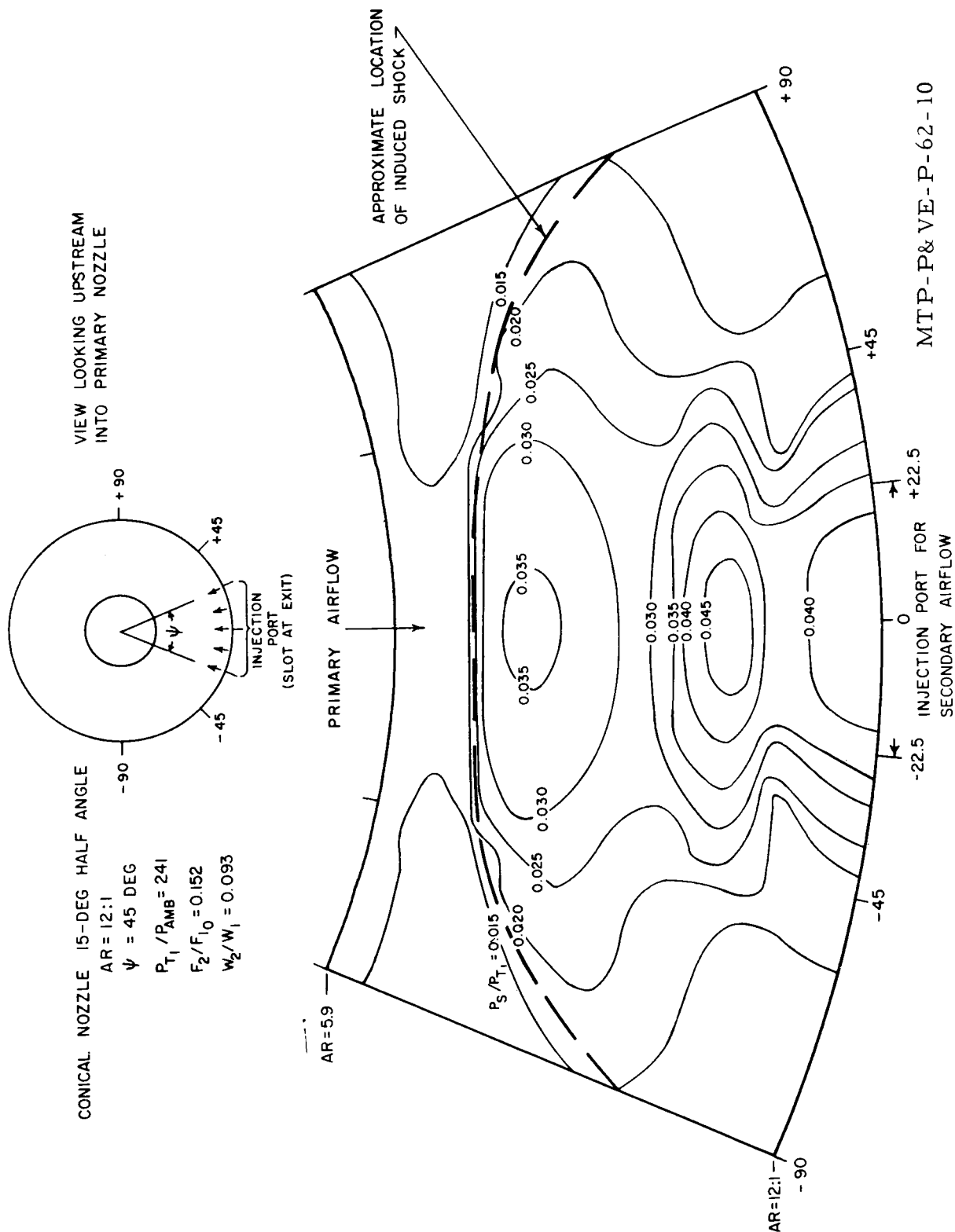


FIGURE 8. PRESSURE DISTRIBUTION ON NOZZLE WALL DURING VECTORING

change of momentum of the secondary gas to the induced side-force through the use of boundary layer separation so as to account for Reynolds number effects (engine sizing) and the effect of three-dimensionality of the injected region.

The analysis includes the effects of primary and secondary gas Mach number, angle of injection, aspect ratio of the injection slot, and gas properties of the injectant (molecular weight, temperature, and ratio of specific heats).

ANALYTICAL EXPRESSION FOR SIDE-FORCE

The performance computed by the analysis results in a nonlinear relationship between the side force and secondary injection mass flow rate. Referring again to FIG 5, the analytical expression to calculate side-force can be written:

$$F_2 = (\phi_r + C_f \phi_i) V_2 \dot{W}_2 \quad (2)$$

where:

F_2 = side force, lb

ϕ_r = reaction term, sec^2/ft

$C_f \phi_i$ = induced term, sec^2/ft

$V_2 \dot{W}_2$ = momentum of secondary flow, $\frac{\text{ft lb}}{\text{sec}^2}$

The various terms in the equation C (2) have this significance:

1. The parameter ϕ_r accounts for the component of the secondary jet reaction force which acts in the desired lateral direction.
2. The parameter C is a measure of the efficiency of the induced pressure field in producing a side-force in the desired lateral direction.

(This term results from the lateral spreading of the interaction region to the sides of the nozzle where the incremental pressure-area force is not parallel to the desired direction.)

3. The parameter f is a ratio of the total induced pressure force on the nozzle walls to the pressure force which acts on the secondary jet, turning it rearward. The term is evaluated with the aid of boundary layer separation criteria.

4. The parameter ϕ_i is a measure of the change in axial momentum of the secondary jet. The magnitudes of c , f , and ϕ_i can be evaluated either experimentally or theoretically. Note that this method of analysis is not limited in any of the following ways:

- a. The iteration model to which it can be applied is flexible.
- b. The separation criterion may vary.
- c. Primary and secondary nozzle contours may vary.

Equation (2) may be expressed in the following terms:

$$\frac{F_2}{F_1} = \frac{\left[Cf \left(\frac{V_2}{a^*_2} \sin \alpha + 0.9 \right) + \left(1 + \frac{1}{\gamma M_2^2} \right) \frac{V_2}{a^*_2} \cos \alpha \right] \times \frac{a^*_2}{a^*_1} \times \frac{\dot{W}_2}{\dot{W}_1}}{V_1 / a^*_1} \quad (3)$$

This may be rewritten to:

$$\frac{F_2}{F_1} = \frac{\left[\left(\frac{Cf}{f_{2D}} \right) f_{2D} \left(\frac{V_2}{a^*_2} \sin \alpha + 0.9 \right) + \left(1 + \frac{1}{\gamma M_2^2} \right) \frac{V_2}{a^*_2} \cos \alpha \right] \times \frac{a^*_2}{a^*_1} \times \frac{\dot{W}_2}{\dot{W}_1}}{V_1 / a^*_1} \quad (4)$$

See Appendix II for the derivation of equation (3).

A sample calculation using equation (4) and the data from the figures included in the report is included in Appendix II.

COMPARISON OF EXPERIMENTAL AND THEORETICAL DATA

A comparison of experimental data with theoretical calculations employing this method is shown in FIG 9, 10, and 11. FIG 9 shows both the lateral and axial amplification factors as a function of the angle of upstream injection. Theory and experiment show that the lateral amplification factor increases with increasing angle of injection, reaching a maximum for an angle of approximately 40 degrees.

The effect of increasing weight flow (spreading of interaction region) is taken into account by the decrease of the term:

$$\frac{C_f}{f_{2-D}}$$

NOTE: 2-D means two-dimensional.

where f_{2-D} is the value for a two-dimensional separation model.

It should be noted that the improved lateral performance (with increasing α) is accompanied by a reduction in the axial amplification factor. In evaluating the performance of secondary injection systems, both lateral and axial performance must, of course, be considered.

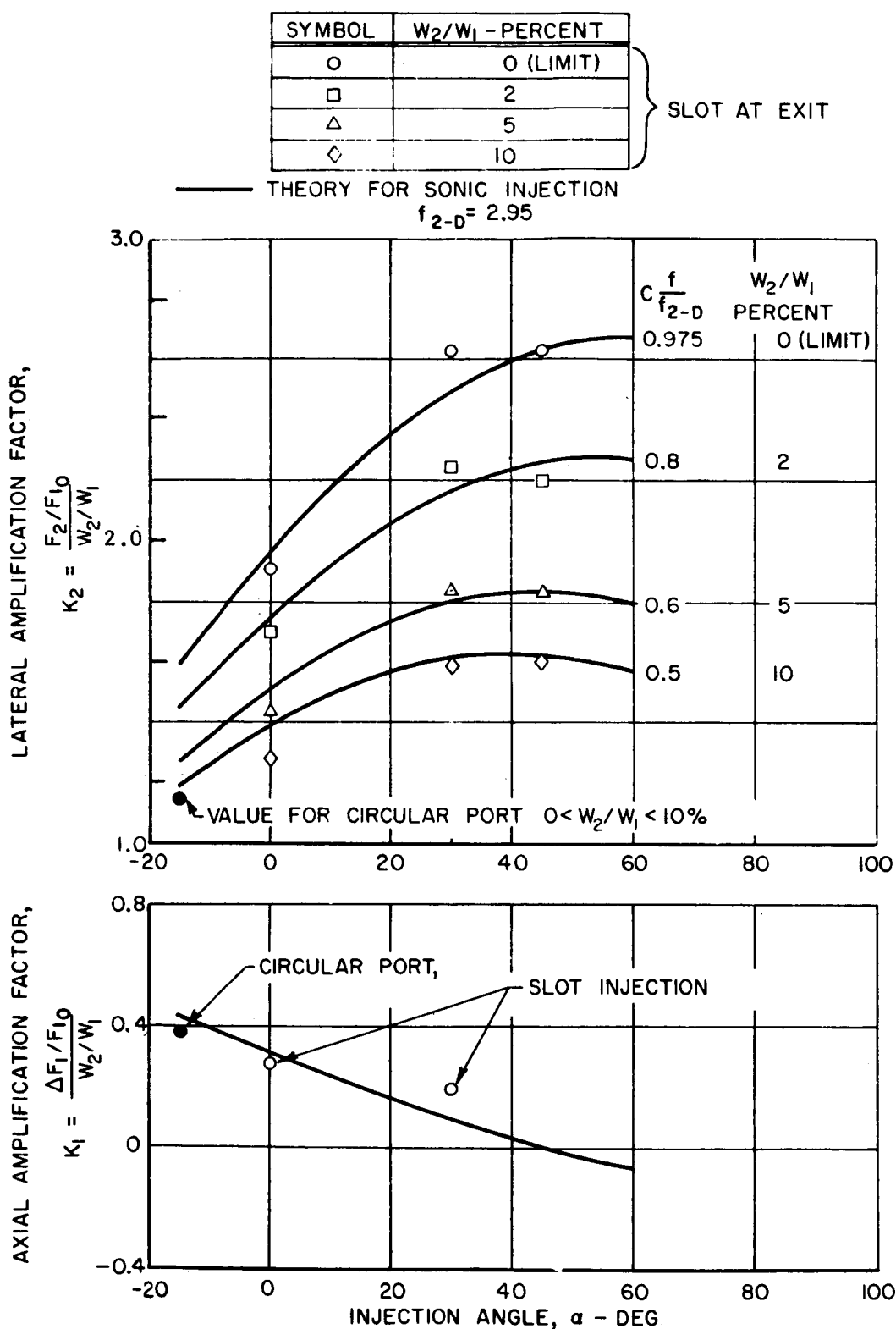
FIG 10 shows the effect of primary nozzle area ratio on the lateral amplification factor for two configurations:

1. Injection through a circular sonic port.
2. Injection at exit through a circumferential slot.

For both areas the secondary injection performance is insensitive to primary nozzle area ratio over the current range of interest of rocket nozzles.

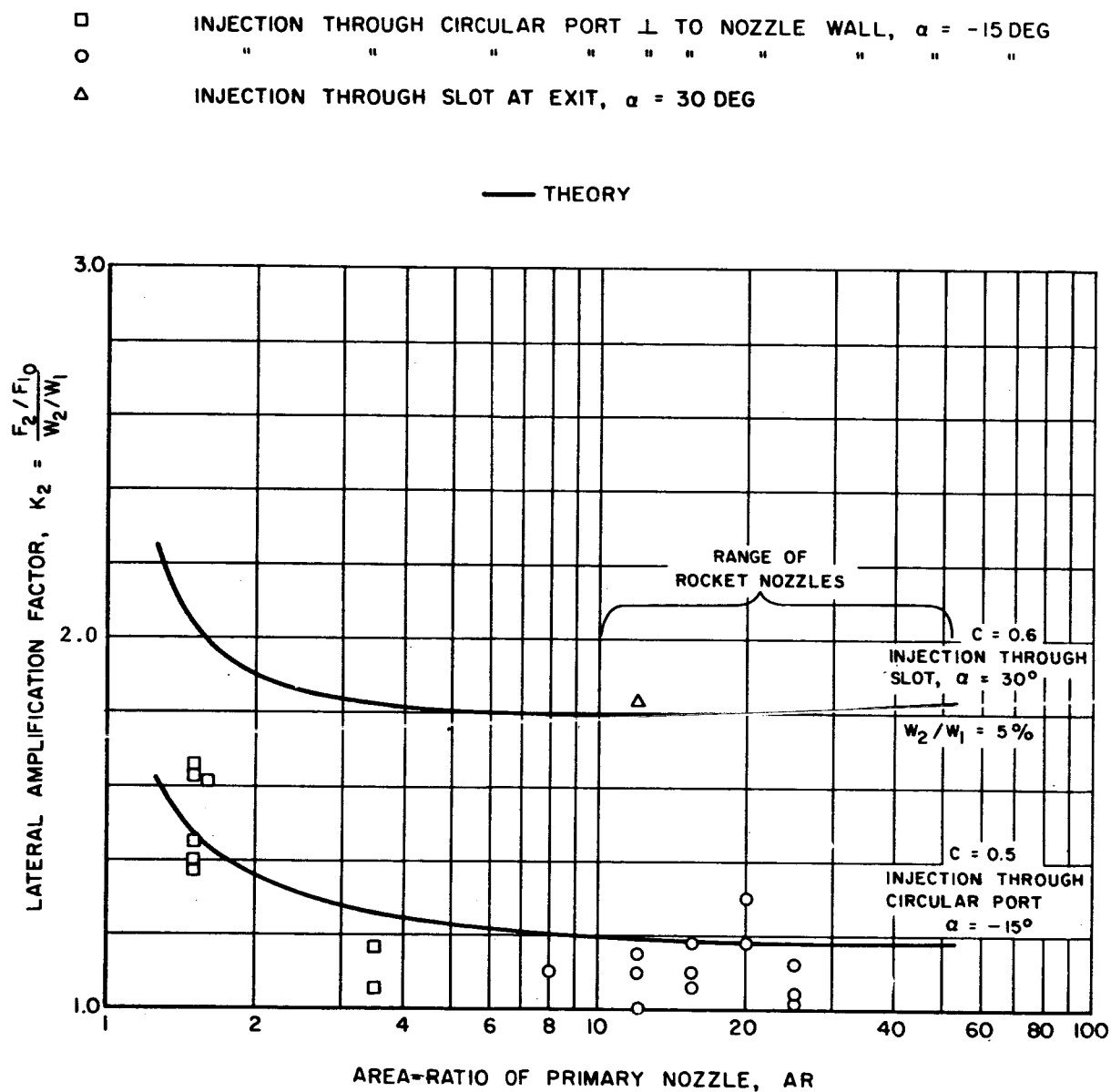
FIG 11 shows the effect of the secondary injection Mach number for three injection configurations:

1. A circular port.



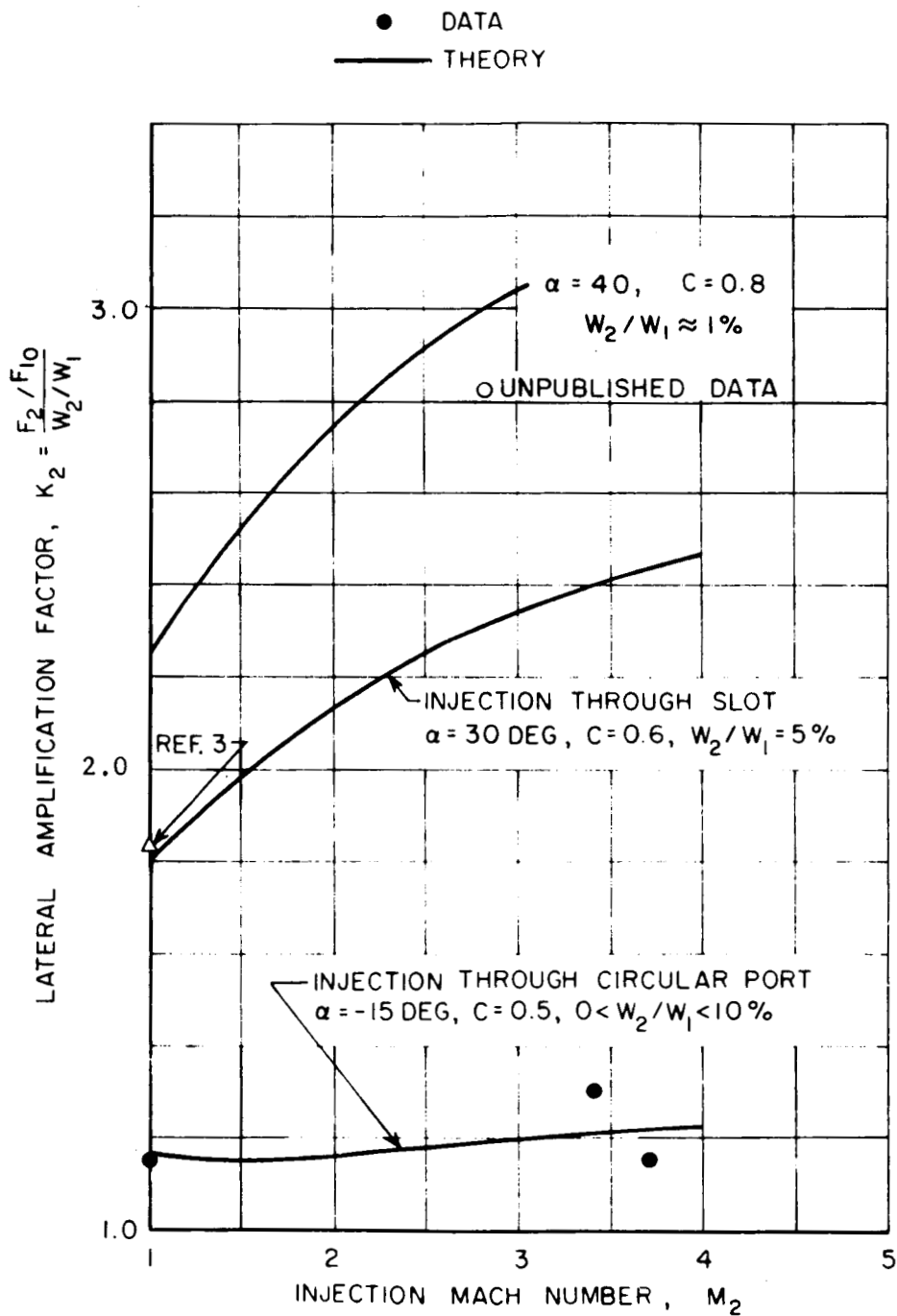
MTP-P&VE-P-62-10

FIGURE 9. VARIATION OF LATERAL AMPLIFICATION FACTOR
WITH INJECTION ANGLE



MTP-P&VE-P-62-10
 FIGURE 10. VARIATION OF LATERAL AMPLIFICATION FACTOR WITH PRIMARY NOZZLE AREA RATIO

CONICAL PRIMARY NOZZLE, AREA RATIO = 12:1



MTP-P&VE-P-62-10

FIGURE 11. VARIATION OF LATERAL AMPLIFICATION FACTOR WITH INJECTION MACH NUMBER

2. A 30-degree slot with 5 percent secondary weight flow.
3. A 40-degree slot with 1 percent secondary weight flow.

The theory and experiment are in general agreement.

CORRELATION OF HOT-FLOW AND COLD-FLOW DATA

The preceding discussions were based on data obtained from tests employing room-temperature air for both the primary and secondary streams, i. e., a homogeneous model. The validity of these data in predicting the performance of a rocket nozzle employing hot gases other than air in which the primary and secondary gas is not the same, i. e., a heterogeneous model, has been studied. A relatively simple correlation term has been developed which appears to work quite well. The term is:

$$\sqrt{\frac{M_1}{M_2} \times \frac{T_{T_2}}{T_{T_1}}}$$

where M is the molecular weight and T_T is the stagnation temperature.

It is apparent that the lower the molecular weight and the higher the temperature relative to the main nozzle flow, the better the injectant's performance.

Equation (3) may be written:

$$\frac{F_2}{F_1} = K_1 \times \frac{\dot{W}_2}{\dot{W}_1} \quad (5)$$

In the equation K_1 is called the amplification factor.

Equation (5) may be written to include the correlation term as follows:

$$F_2 = K_1 \sqrt{\frac{M_1}{M_2} \times \frac{T_{T_2}}{T_{T_1}} \times \frac{W_2}{W_1}} \quad (6)$$

The corrected amplification factor K_2 is then defined as:

$$K_2 = K_1 \sqrt{\frac{M_1}{M_2} \times \frac{T_{T_2}}{T_{T_1}}} \quad (7)$$

As an example of the effect of the correlation term on the corrected amplification factor, let us consider an air-to-air amplification factor of 2.9 and the following:

Injectant is hydrogen, at combustion chamber temperature ($H_2 - O_2$ engine, $O/F = 5.5$):

$$\begin{aligned} \text{Then} \quad M_1 &= 2 \\ T_{T_1} &= T_{T_2} \\ M_2 &= 13 \end{aligned}$$

$$K_2 = K_1 \sqrt{\frac{M_1}{M_2} \times \frac{T_{T_2}}{T_{T_1}}}$$

Substituting:

$$K_2 = 2.9 \sqrt{\frac{13}{2} \times 1}$$

$$K_2 = 2.9 \times 2.55 = 7.395$$

At equal temperatures, the strong effect of molecular weight on the amplification factor is quite apparent.

It is this factor that makes hydrogen an ideal injectant.

ENGINE-INTEGRATED SECONDARY INJECTION SUBSYSTEM

Certain desirable qualities of an engine-integrated secondary injection subsystem are apparent:

1. Sustained high engine specific impulse during and without secondary injection.
2. No objectionable dynamic coupling or instability as a result of diverting main propellants (or hot gas) from the basic engine for secondary injectants.
3. No adverse chamber cooling problem induced by the secondary injection mechanism.
4. A minimum of added controls and flow circuits (operating unreliability and leakage sources).
5. Fail-safe features such that there is a high probability that a failure in the injection subsystem will not produce an overall engine malfunction, nor seriously degrade its performance.

It is apparent from the above that if secondary injection is to be employed in a conventional rocket engine, it cannot be considered merely as auxiliary equipment to be "added on" as is--for example--a measuring instrumentation kit. Instead it is, and must be handled as, a distinct subsystem of the engine. Hence, it must follow the same strictly controlled development and qualification procedures which the turbopump, engine controls, and thrust-chamber subsystems themselves undergo. In short, from the start it must be viewed as a vital part of the engine-flow circuit.

The optimal injection configuration for hot gas secondary injection in a hydrogen-fueled engine has not yet been established. In all likelihood, especially as hardware practicability considerations are introduced, there will be some variation from engine to engine in the particular configuration chosen.

Side-force generation by means of secondary fluid injection in the nozzle of a rocket has been accomplished (or proposed) with many

variations in both the nature and source of the fluid used, and in the mode and configuration of injection. In Table 1 an attempt has been made to identify those key variables which can be used to completely characterize any secondary injection scheme. For convenience, systemization to the extent of coding these variations for quick identification of any given system configuration is readily accomplished. Further consideration of this point is outside the scope of this report, however.

Referring again to Table 1, the important variables remaining to be defined for selection in the hot gas secondary injection version are:

1. Mode of fluid control
2. Injection plane(s) location along the nozzle
3. Injection angle
4. Injection port configuration
5. Injection velocity

Point 1, the mode of fluid control, may be pretty much settled by the system approach chosen; i.e., auxiliary combustor, chamber tap, etc. This point will be discussed later in this section. The remaining four variables (points 2-5) are--in the first analysis--determined by performance considerations. It is in this area that the NASA-supported work at the UAC Research Laboratories cited earlier is expected to be especially relevant. Fortunately, the engine secondary injection subsystem can be viewed in considerable detail without waiting for selection of a specific injection configuration. It follows that hardware-level engineering activity on an engine-integrated secondary injection system can be entered upon profitably now. Some possible approaches in establishing a secondary injection configuration are described in the following section.

For a typical turbopump-type, regeneratively cooled, hydrogen-oxygen engine there appear to be several feasible approaches for

Table 1. Outline of Variables for Secondary Injection
Side-Force Generation

1	Fluid Type	Liquid	Monopropellant Non-Reactive Reactive	
		Gas	Cold $0^\circ < T < \text{Amb}$ Hot $\text{Amb} < T$	Non-Reactive Non-Reactive Reactive
2	Fluid Source		Main Propellant(s) Auxiliary (3rd) Propellant Fluid	Fuel Oxidizer Bipropellant
		Turbine	Main Combustion Chamber Exhaust	
3	Fluid Control		No. of Control Points	1, 2, 3, 4, n
			Type	Off-On Discrete-Steps Continuously Variable
			Valve Actuation	Electromechanical Pneumatic Hydraulic Aerodynamic
4	Injection Plane Location		Throat, $\frac{A_i}{A_t} = 1$	
			Nozzle, $1 < \frac{A_i}{A_t} < \epsilon$	
			Exit, $\frac{A_i}{A_t} = \epsilon$	
5	Injection Angle		Downstream, $0^\circ < \alpha < 90^\circ$ Normal, $\alpha = 90^\circ$ Upstream, $90^\circ < \alpha < 180^\circ$ Note: α Measured Relative to Nozzle Centerline	
6	Injection Port Configuration		Unitary (Small Port) Multiple (N per control point & angle covered) Probe-in-Stream Other	
7	Injectant Velocity		Sub-sonic, $M < 1.0$ Sonic, $M = 1.0$ Supersonic, $M > 1.0$	

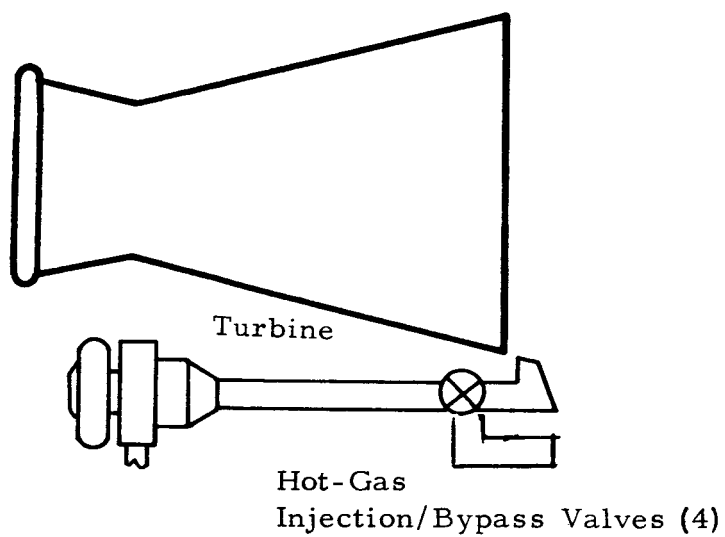
mechanizing the hot gas injection system. As discussed earlier, for this application, hot gas injection appears to be markedly superior in performance to cold gas or liquid injection. Therefore, only hot gas injection will be further discussed here.

For illustrative purposes, five basic injection methods are described below. These differ fundamentally in only one respect: the source of hot gas injectant. This difference has a dominant effect on the hardware implementation situation. We emphasize that the methods described herein are not necessarily optimal. First-order analysis has indicated, however, that they are among the more promising proposals.

1. Turbine Exhaust Utilization (FIG 12a)-Turbine exhaust gases are already at a relatively moderate temperature (turbine limitation) and hence should normally require no further hydrogen dilution. The gas is routed to the secondary injectant control points and is controlled by valves, similar to those described under 2 below. Since pressures are comparatively lower (higher specific volume), the ducting and valves will be physically larger. In addition, a means must be provided to permit normal exhaust passage when secondary injection is not being performed. Spring-loaded relief valves in the exit manifold have been proposed for this purpose (Aerojet).

An interesting alternative approach here (FIG 12b) involves the use of a multiplicity of Bi-Stable "Aerodynamic" valves (in place of standard nozzles) which either inject gas into the nozzle to create side-force, or dump the gas overboard normally. Both UAC and TAPCO have developed such devices. This approach may be especially applicable to engines with turbine exhaust-cooled skirts, such as the M-1.

2. Combustion Chamber Tap with Hydrogen Dilution (FIG 12c)-Hot gas is routed on demand from the main combustion chamber and is immediately mixed with hydrogen to reduce its temperature (and to lower its mean molecular weight). The gas routed to the secondary injectant points and injection is controlled by high-response hot-gas valves, one at each control point.



Turbine Exhaust Utilization

FIGURE 12a

(NOTE: FIG 12b
on next page)

MTP-P&VE-P-62-10

Turbine Exhaust
Inlet & Manifold

Exhaust-Gas
Cooled Skirt

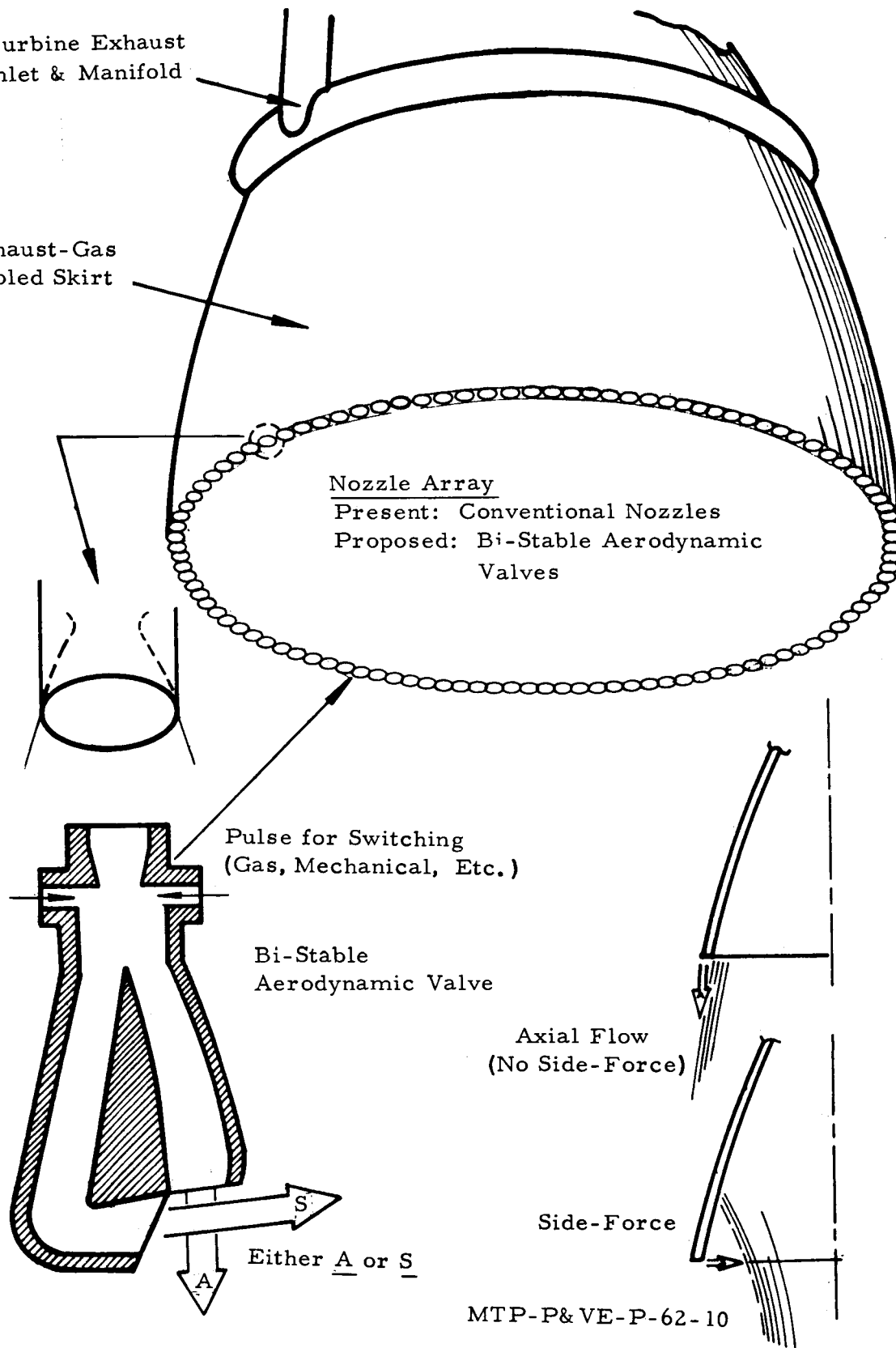
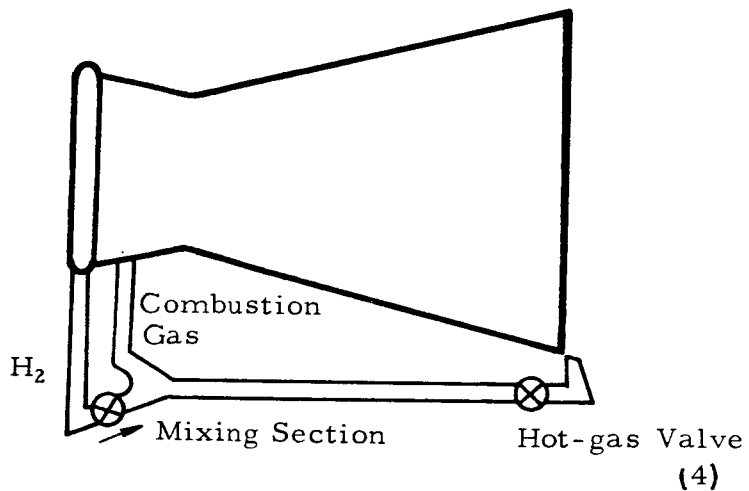
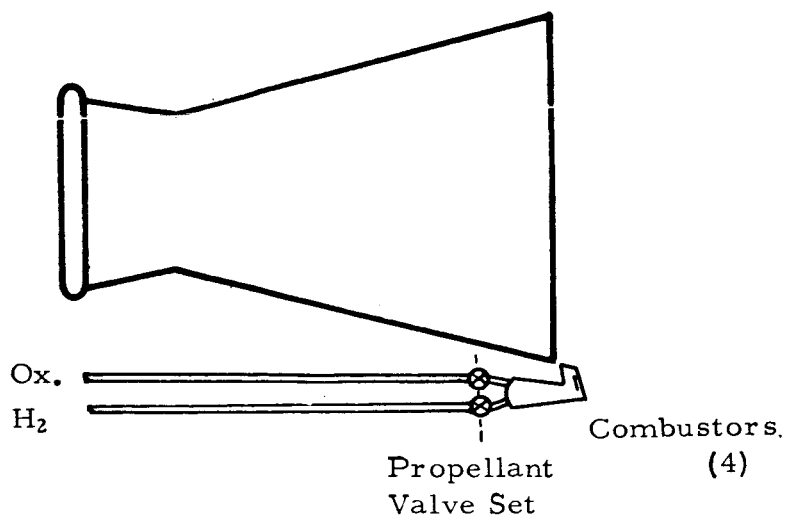


FIGURE 12b. ALTERNATIVE TURBINE EXHAUST
UTILIZATION SCHEME



Combustion Gas with Hydrogen
Dilution

FIGURE 12c



Auxiliary Combustion Devices

FIGURE 12d

3. Demand-Type Auxiliary Combustors (FIG 12d) - Hydrogen and oxygen high-pressure feed lines are tapped to provide propellants for the operation of gas-generator type combustion devices at each of the secondary injection points (normally four). Propellant flow control is via a high-response, proportional-type throttling valve for both propellants at each location. A common actuator for these two valves is possible.

4. Hydrogen Dump Cooling (FIG 12e) - Development has begun on one type of non-regeneratively cooled thrust-chamber of interest. The technique referred to has been termed hydrogen dump-cooling. In this type of chamber a small amount of the total engine hydrogen flow (a few percent) is passed into a cooling passage around the thrust chamber combustion liner for cooling purposes. This heats the hydrogen considerably. It is then "dumped" through an expansion nozzle(s) at the lip of the nozzle exit. This hot hydrogen flow produces thrust at fairly high specific impulse. Several significant advantages over conventional regenerative cooling have been cited for this scheme.

This particular prospect is mentioned here because it may result in a situation directly amenable to secondary-injection with hot hydrogen, which is highly desirable performance-wise. The possibility of using a bypass type system in the nozzle to obtain hot hydrogen injection in conjunction with the axial thrust recovery nozzles is indeed an interesting prospect. Perhaps the bi-stable aerodynamic valve discussed earlier is applicable here also.

5. High-Temperature Hydrogen Injection (FIG 12f) - Ultimately, for very high performance secondary injection systems, analysis has clearly indicated the advantages of injecting pure hydrogen at as high a temperature as possible. The previous section has indicated the side specific impulse values obtainable. The accompanying sketch represents this approach, leaving open the selection of a source of the requisite highly-heated hydrogen. Several candidate approaches have been suggested: High-energy-release heaters, vortex-type hydrogen separation devices, and ultra-high efficiency heat-exchangers. Of course, the nuclear rocket would likely use heated hydrogen tapped from the reactor.

The first three of these five approaches, since they are closer to an operational status, are outlined further in the accompanying table (Table 2).

Table 2. Characteristics of Three Secondary Injection Sub-System Approaches

Reference Figure in Report	I Turbine Exhaust 1. Bypass System	2. Bi-Stage Aerodynamic Values	II Combustion Chamber Tap	III Demand-Type Auxiliary Combuster
	FIG 12a	FIG 12b	FIG 12c	FIG 12d
Source of Hot Gas	Turbine Exhaust	Turbine Exhaust	Combustion Chamber	Auxiliary Combustors
Additional Propellant Lines (Cold) Required	None	None	Possible Short Length for Dilution H ₂	Feed-Lines to Combustors
Additional Hot-Gas Ducts Required	Ducts and Manifolding at Secondary Injection Location (Possibly minimized with hot-gas skirt)	Ducts and Manifolding at Secondary Injection Location (Possibly Elim. with hot-gas skirt) Bi-stable aerodynamic valve and actuation system	Ducts to Secondary Injection Location	None
Control Devices Required	Hot-Gas Throttling Valve and Bypass Device	Bi-Stable Aerodynamic Valve and Actuation System	Hot-Gas Throttling Valve, and H ₂ Dilution Control	Bipropellant Throttling Valve
Mode of Fluid-System Dynamic Coupling to Engine	Possible Variation in Turbine Exhaust Pressure	Possible Variation in Turbine Exhaust Pressure	Chamber Pressure Perturbation	Feed Line Pressure Perturbation
Basic Limitation	Limited Flows and Pressures Available	Limited Flows and Pressures Available	Interference with Combustion Chamber Conditions	Interference with Propellant Feed Conditions
Critical Item to be Developed	Hot-Gas Valve and Bypass Device	Bi-Stable Aerodynamic valve and Actuation Scheme	Hydrogen Dilution Device and Hot-Gas Valve	Reliable High Response Combuster Including Ignition and Valving Mechanization
Principal Advantage	Uses Gas Normally Dumped Overboard	Uses Gas Normally Dumped Overboard, Control System Advantages (Digital System)	Abundant Hot-Gas Source	No Hot-Gas Valve, Present Technology is Applicable

FIGURE 12e

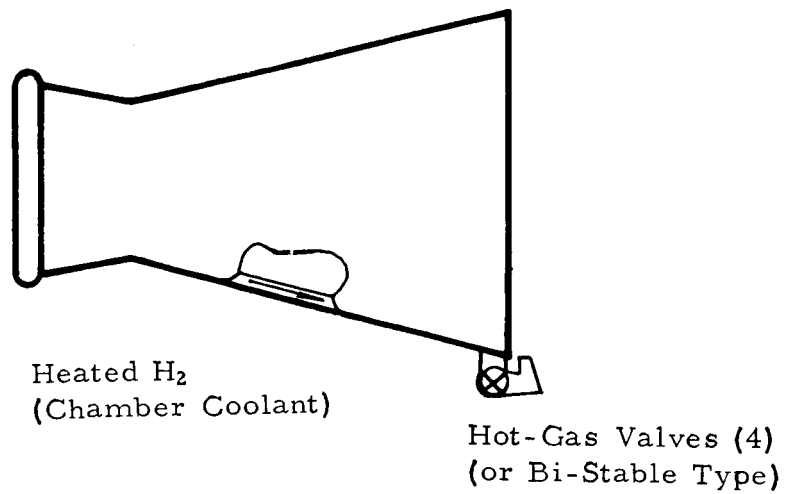
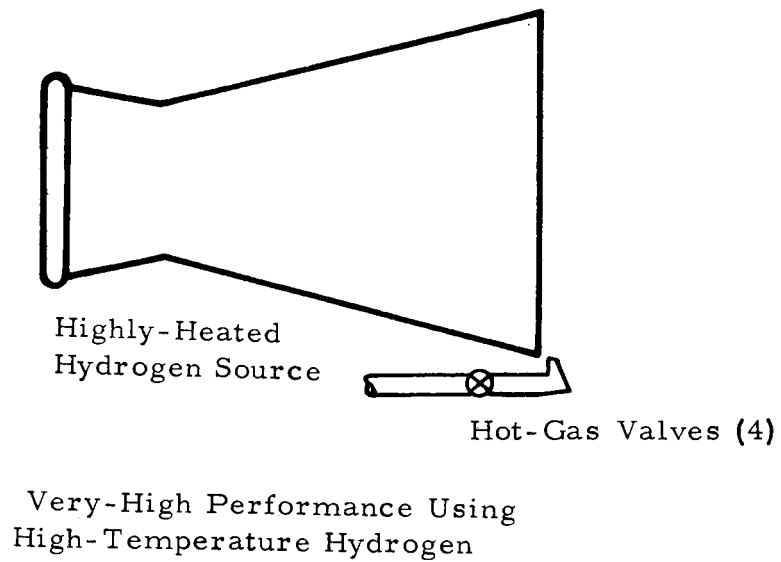


FIGURE 12f



MTP-P&VE-P-62-10

Thrust Chamber Cooling as Affected by Secondary Injection

It is apparent that the supersonic flow in the vicinity of the nozzle wall is drastically changed in the region influenced by secondary injection. A serious question naturally arises: How is heat transfer to the wall affected? This potential problem has several interesting ramifications, such as:

An increase in local heat transfer rates might be expected along, or in the vicinity of the separated/non-separated flow terminator. The postulated reason for this lies in the fact that the boundary layer is torn away from the wall in this area, behind which is formed a re-circulating turbulent zone in which primary (main stream and boundary layer) and secondary gases are mixed. The insulating gas film normally counted on to protect the wall is thus drastically modified. Some evidence of excessive heating rates has been, in fact, reported in rocket engines which experience nozzle flow separation.

A decrease in the over-all heat transfer rates is anticipated since the wall heat input downstream of the separated region should be considerably reduced. One factor here is the influence of the injectant gases which are at a much lower initial temperature than the primary stream. Flow velocities will, in general, be lower behind the separated front.

The mechanism of possible nozzle wall failure from the first point above is readily seen. However, potential problems resulting from the second require additional considerations.

The possible failure mode here is an induced wall burn-out in the nozzle throat region. The reasoning goes as follows: Assuming a tube-wall type thrust chamber, if insufficient heat is transferred into the hydrogen in the nozzle region (i. e., under the separated flow), then the hydrogen temperature and specific volume and hence hydrogen velocity will be considerably subnormal as it passes through the throat portion of the tube. Since tube cooling is critically dependent on coolant velocity, insufficient tube-cooling may then result. Also, as is generally known, the specific heat of hydrogen can be relatively low until it is warmed up in the initial section of the cooling jacket. If, due to secondary injection-induced separation and resulting low heat flux in a sector of the nozzle, this initial warming of the hydrogen

does not take place, then hydrogen with decreased specific heat characteristics may affect cooling in the critical throat region.

There are prospects that some clarification of the potential wall cooling problems may come about in the current UAC Research Laboratory work. General background on separated turbulent boundary layers exists and to a certain extent is applicable to this problem. Definitive experiments with actual thrust chamber hardware types of interest are definitely needed.

VEHICLE CONSIDERATIONS

The relaxation of adverse design restraints which can accompany a shift from a gimbaled to a fixed-engine configuration will be significant in these areas:

1. Elimination of large concentrated steady-state and dynamic reaction loads at the gimbal and actuator engine tie-points, both engine and vehicle.
2. Gross reduction in operating element size and power supply requirements.
3. Marked lowering of transverse acceleration, shock, and low-frequency vibration environment for critical engine components and subsystems such as nozzle skirt, turbopumps, and controls.
4. Elimination of large-displacement deflections in propellant feed lines. The weight and development difficulties of complex linkage-reinforced, pressure-balanced bellows type suction lines are well known. These are also extremely difficult to insulate in a hydrogen line. Their length as established by the angular flexing requirement normally forces the engine to be mounted farther from the propellant tankage than otherwise would be the case (FIG 13).
5. Ability to use a higher nozzle expansion area-ratio in a given diametral envelope, since no clearance is required to accommodate physical excursions. Also a reduction in interstage adapter section lengths, since fixed engines can be moved closer to tank aft dome.

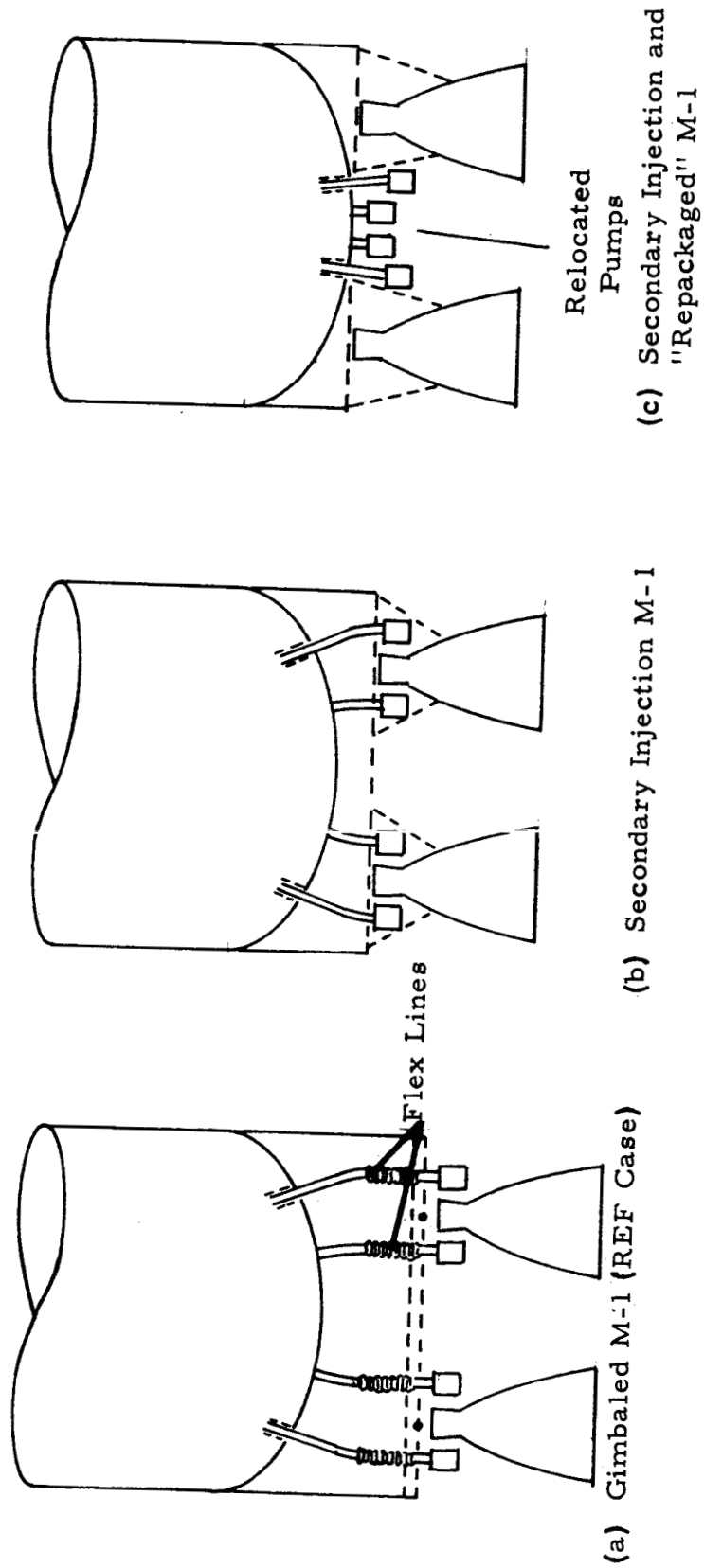


FIGURE 13. COMPARISON OF POSSIBLE POWERPLANT ARRANGEMENTS WITH GIMBALED AND SECONDARY INJECTION VERSIONS OF THE M-1 ENGINE

MTP-P&VE-P-62-10

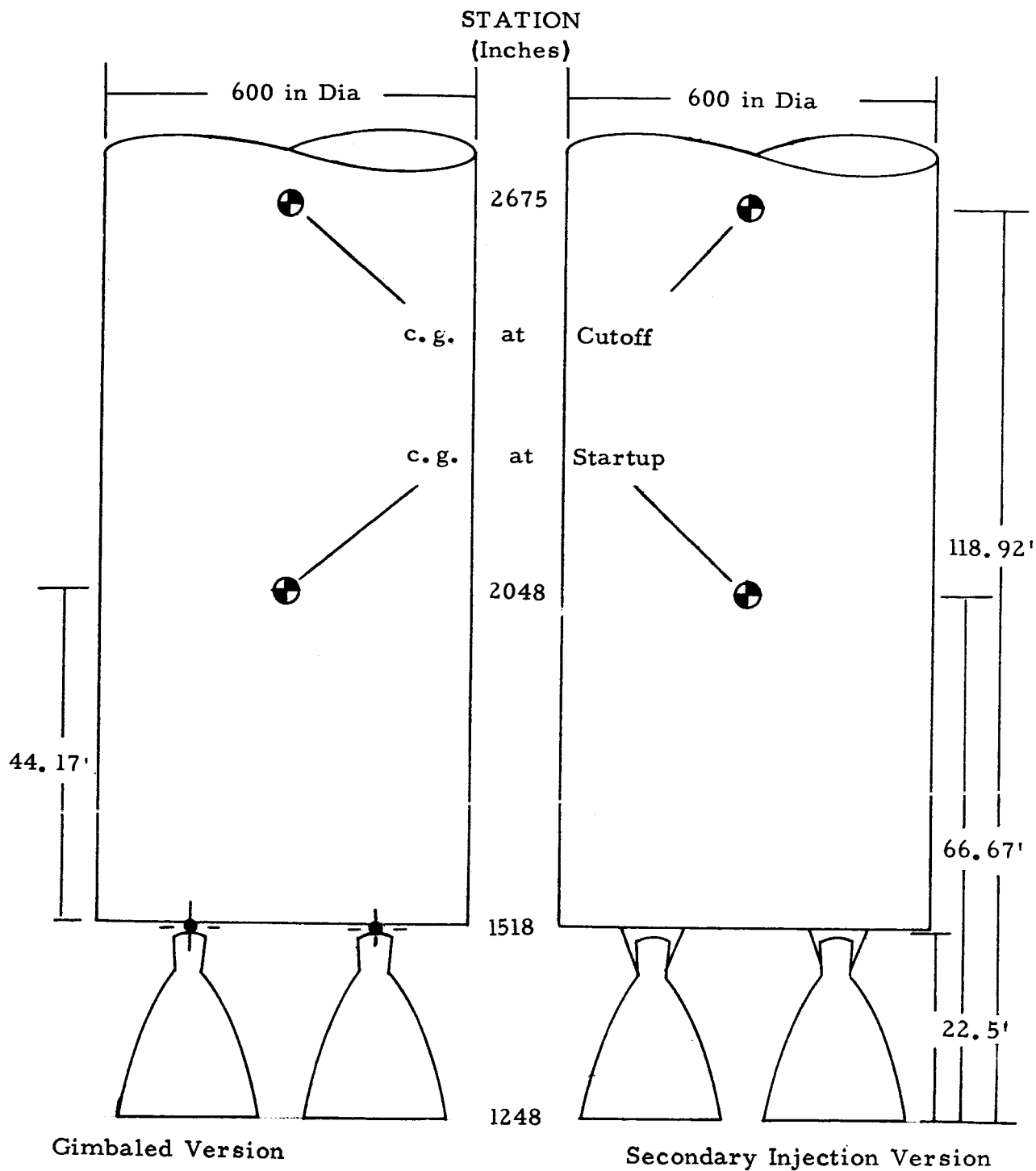
6. Simplification of aft-end heat protection shielding if required, since flexible sections are no longer required.

7. The arrangement and interconnection of engine subsystems and components can be improved in many instances since they no longer have to be "packaged" around the engine toward achieving a static balance and minimum moment of inertia about the gimbal. For example the turbopumps may be more closely grouped and tank-mounted to minimize propellant feed and turbine exhaust line lengths, and to improve cool-down characteristics.

To illustrate some of the major influences on a vehicle in going from a movable to a fixed engine installation, a possible NOVA second-stage configuration (N-II) with two M-1 engines was studied in three versions. The first (A) utilizes the present gimbale M-1 engine concept. It serves as a reference case for the remaining two cases, both of which employ fixed engines. Although side-force generation via secondary injection using turbine exhaust gases was assumed, details of the subsystems for providing this were not included in the study. Version B retained the present engine configuration as is, but shifted the thrust transmission point from the gimbal to the thrust chamber skirt, i. e., from a concentrated to a distributed load path to the vehicle. Version C used a similar thrust chamber attachment approach, but had in addition a rearrangement of engine components. Principally this consisted of a re-grouping of the turbopumps to somewhat reduce engine weight and to permit simplification of the suction line and insulation arrangement. Versions A, B, and C are shown in FIG 13a, 13b, and 13c, respectively.

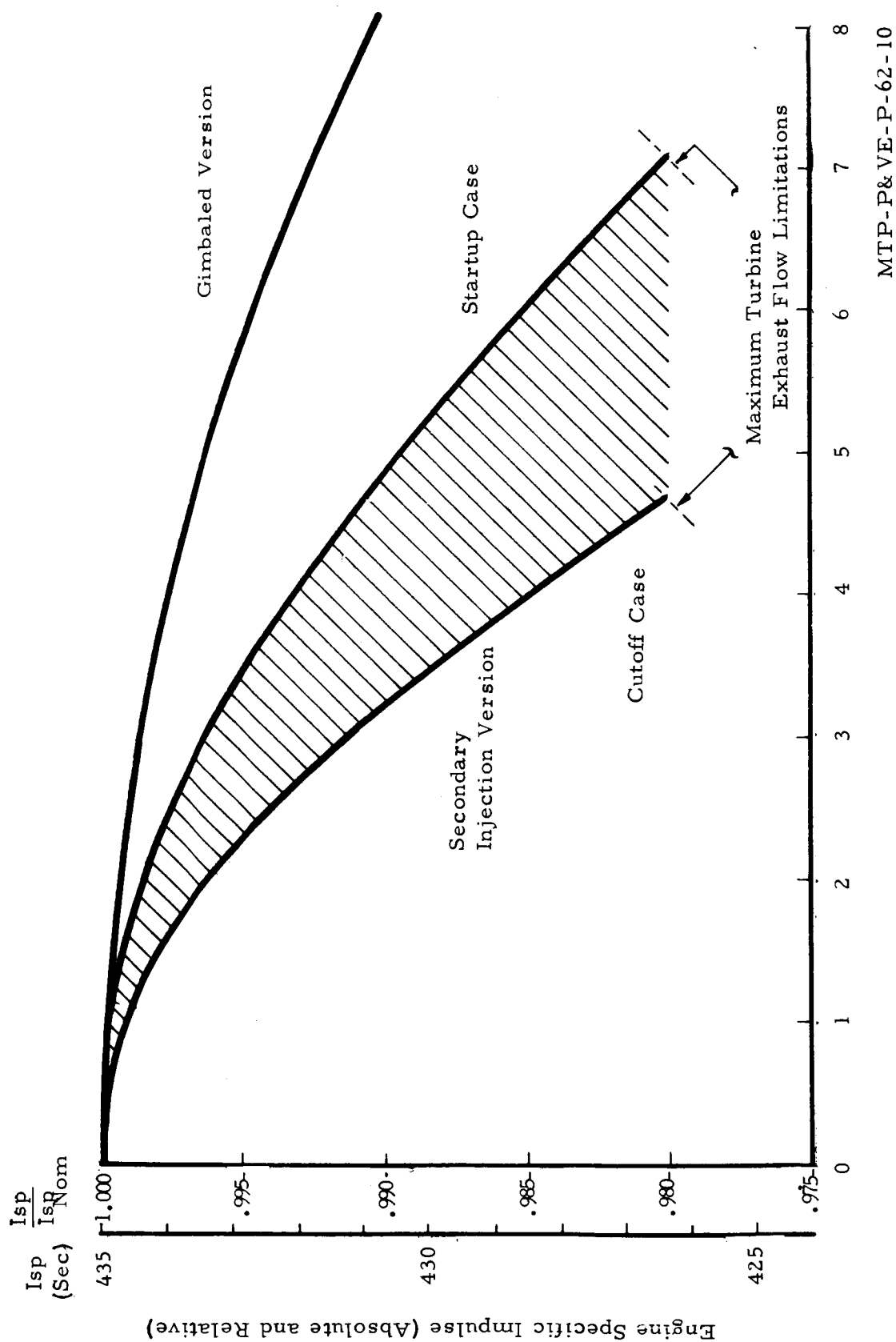
Originally it had been our objective to present a comparison of the payload capabilities of each of these configurations. This was to be done essentially through supporting (weight and performance--specific impulse) studies.

The latter of these was accomplished for a particular case which is illustrated in FIG 14 and 15. (See Appendix III for this analysis). As can be seen, the relative performance loss of the secondary injection configurations as compared to the gimbaling case becomes significant only at sizeable effective line-of-thrust deflections. For example, at an effective deflection of 6 degrees the gimbale vehicle betters the secondary injection vehicles by over 4.0 seconds



MTP-P&VE-P-62-10

FIGURE 14. GIMBALED AND SECONDARY INJECTION VERSIONS
OF MODEL M-1 STAGE



EFFECTIVE GIMBAL DEFLECTION ANGLE - DEGREES

FIGURE 15. ENGINE SPECIFIC IMPULSE VERSUS EFFECTIVE GIMBAL ANGLE

of specific impulse on a nominal engine basis of 435 seconds.* At smaller effective deflection angles, which may realistically characterize the mean "over-the-burning-period situation" expected -- say, a 1 degree deflection -- the two configurations differ by considerably less than 1 second.

So, it appears there is no significant performance advantage for either the gimbaling or secondary injection approach. Again, the opportunity of going to a higher nozzle expansion area ratio which the fixed engine permits was not exploited in this study.

Noting then, the equivalent specific impulse performance of this comparison case, payload differences would be solely a function of stage mass-fractions: here, the salient advantage of the fixed engine is felt to exist.

A cursory structural analysis did indicate that a weight saving accompanied the shortening of the powerplant. This possibility exists with the fixed-engine configurations, primarily because of the extended length of the gimbaled engines' flexible propellant ducts. An interstage shortening of as much as 100 inches (out of a total of about 850 inches) appeared practical. Depending on what portion of the interstage remains with the second-stage through its powered flight, this may or may not be a substantial weight savings.

However, other avenues of weight reduction made possible with the fixed, distributed thrust transmission mounting of the secondary injection configurations could not be explored. These required fairly detailed preliminary structural design analysis. Such was necessarily considered outside the scope of this investigation.

Summarizing, then, for the particular vehicle cases investigated, there appears to be little difference of specific impulse between a gimbaled version and a secondary injection version. Opportunities for structural weight reduction would seem to accompany the fixed-engine, secondary injection case; however, detailed stage structural design work would have to be started to qualify the performance gain resulting. As stated before, this work was not performed for this report.

*This value is not that officially specified for the M-1 engine.

SOME COMPARATIVE POINTS: SECONDARY INJECTION VIS A VIS GIMBALING

In a manner of speaking, the secondary injection configuration is the challenger; the gimbale engine, the challenged. The question is, are the net advantages of secondary injection over gimbaling only marginal--or are they really significant? To permit an examination of this question in perspective, a point-by-point comparison of the two approaches is appropriate. The discussion which follows attempts to do this on several major comparison points.

1. Equipment Complexity

It is instructive to consider the relative complexity introduced into the basic engine component inventory by the inclusion of a side-force generation system. This, coupled with the more general effect on the stage configuration, should provide an overall index of complexity which will be useful in estimating such things as checkout and instrumentation requirements, and operative reliability expectations.

Gimbaling configurations have, by and large, been standardized to include three major items: Two gimbaling actuators, and a gimbal bearing block. The actuators are usually of the extend/retract type and operate about a nominal stroke mid-point (engine centered). There are also the passive load-carry struts and tie-points which locate the actuators' line-of-force and distribute the actuation loads into the chamber. Reference is made to FIG 16a.

As might be expected, there has been little standardization applicable to gaseous secondary injection devices. Nor is such a standardization really feasible until an engineering consideration of specific systems is entered upon. This last point should be emphasized here--as elsewhere in this report--since hardware-level engineering study can become meaningful only when associated with a realistic engineering view of the secondary injection subsystem.

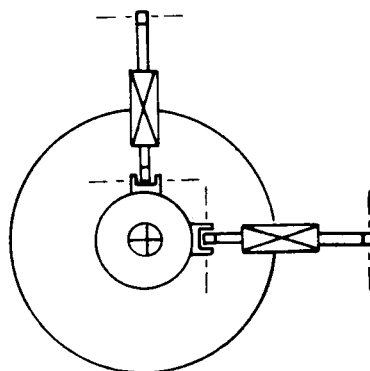


FIGURE 16a

Nevertheless, some of the basic configurations for secondary injection considered thus far in this report lend themselves to at least superficial hardware considerations. The object here then is to present the number and types of components which might be expected in a secondary injection subsystem.

Basically, we have viewed three hot-gas supply configurations (FIG 15 and Table 2) as practical; this acceptance being based on present state-of-the-art hardware technology. These are:

1. Turbine exhaust utilities
2. Combustion chamber tap with hydrogen dilution
3. Auxiliary combustors

In a given secondary injection application, the number of injectant control points and operating elements (hot-gas valves, bi-propellant valves, etc.) is somewhat arbitrary. For the purpose of the following discussion, four control points will be assumed in most cases with injection taking place in each of four symmetrical quadrants (FIG 16b). This basic configuration (and, it is believed, a likely one) will aid comparison with the conventional gimbal layout which is similar from the geometry standpoint.

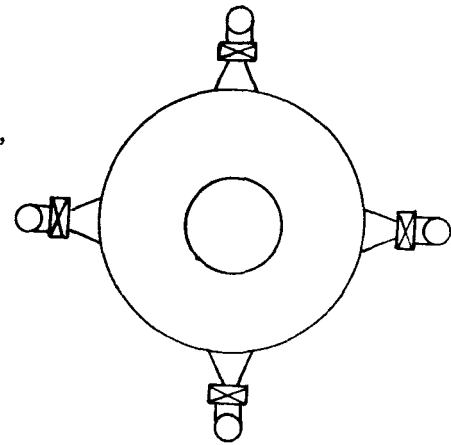


FIGURE 16b

Referring again to FIG 16a through 16d a tentative component inventory for the three hot gas supply system listed above can be posed:

Turbine Exhaust Utilization (Figure 12a)

Hot-gas injectant valves	4
Hot-gas bypass valves	
(Possibly relief-type)	1-4
Total operating elements	5-8

Lines Required: Short, low-pressure hot gas

Combustion Chamber Tap (Figure 12c)

Hot-gas injectant valves	4
Proportional hydrogen	
dilution control unit	1
Total Operating Elements	5

Lines Required: Long, high-pressure hot gas

Auxiliary Combustor (Figure 12d)

Bipropellant valve sets	4
Combustor and ignition devices	$\frac{4}{8}$
Total operating element	8

Lines Required: Long, high-pressure propellant (Small diameter)

The number of operating elements can possibly be reduced by making the individual elements more versatile. For example, if a bi-linear (that is, plus-zero-minus) valve is employed to control the flow to opposing injectant stations, then two valves (not four) would suffice (FIG 16c). Further, if a combined "four-way" valve could be devised (FIG 16d) then the number of basic operating elements might even be reduced to one. But a reduction in quantity is bought at the expense of design complication of the operating element. In addition, remote siting of the operating element from the injection point perhaps could result in increased line lengths. So, the advantage of these combined operations over the four simpler devices is doubtful. Certainly specific system design requirements must be studied before one could rationally choose an approach.

Summarizing, then, the gimbaling subsystem will probably remain somewhat simpler than a secondary injection subsystem in terms of engine operating elements (three, versus five-to-eight, or more elements). Yet, over-all engine simplification--and certainly vehicle simplification as well--will be possible in going from a movable to a fixed-engine installation. The prospective elimination of the difficult-to-insulate hydrogen flex lines is an example of this.

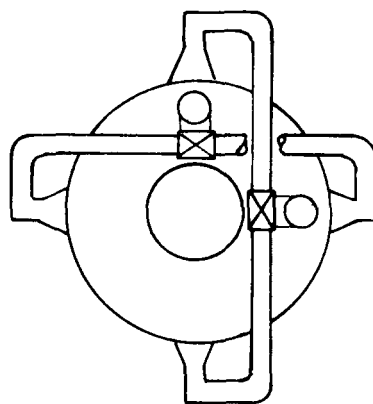


FIGURE 16c

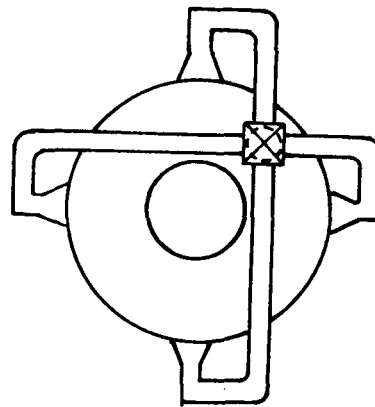


FIGURE 16d

2. Point of Side-Force Application

One important geometric distinction between the mechanism of side-force generation by engine gimbaling and secondary injection is apparent. This is the location (relative to vehicle mass-center) of the applied side force. As represented in the following figure (FIG 17) the gimbal induced side-force is applied at the gimbal block, a distance L from the vehicle center of mass. Secondary injection induced side-force, on the other hand operates farther aft at a distance of $L + d$, where d , in many cases, approaches the full thrust-chamber length.

For the same side-force-induced correction moment a lower; absolute side-force magnitude is required for a secondary injection configuration. This is indicated by the following:

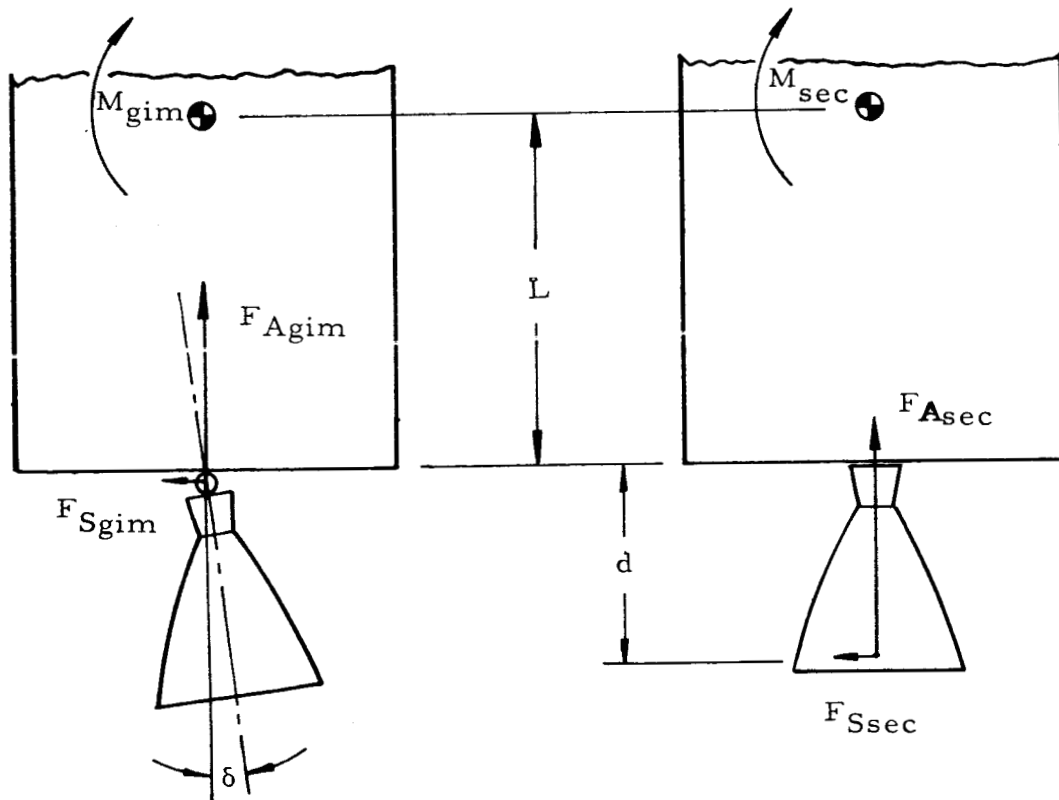


FIGURE 17. COMPARISON OF POINT OF SIDE-FORCE APPLICATION BETWEEN GIMBALED AND SECONDARY INJECTION CASES

Let M = Correction moment about vehicle mass-center
resulting from side-force

F = Engine-developed force

L = Centerline distance from vehicle mass-center to gimbal
block (or forward end of engine)

d = Centerline distance from forward end of engine to
centroid of action of secondary-injection-induced
side-force

δ = Gimbal deflection angle (in plane of figure)

SUBSCRIPTS

s = Refers to side direction, normal to axial reference

g = Refers to gimbaled case

si = Refers to secondary-injection case

$$M_g = F_g \sin \delta \cdot L = F_{sg} \cdot L$$

$$M_s = F_{ssi} \cdot (L + d)$$

For equivalent side-force moments, i. e., for $M_g = M_s$

$$F_{sg} \cdot L = F_{ssi} \cdot (L + d)$$

$$F_{ssi} = F_{sg} \frac{L}{L + d}$$

This relative reduction in side-force magnitude for the secondary injection case becomes quite significant in the case of low length-to-diameter ratio stages, such as the hypothetical Nova-class upper stage viewed here.

3. Response in Side-Force Generation

Let us briefly--and qualitatively--review the comparative mechanics involved in going from a zero side-force condition to a discrete side-force level, in both the gimbaled engine and secondary injection arrangements. Assuming that a step-function command is received, the following transpires:

Gimbaled Engine - Upon command, the mechanical bi-directional actuator rapidly develops a high thrust (or torque) which acts to accelerate the relatively large mass moment of inertia of the engine against bearing and flex-line friction. This angular acceleration is typically limited to about the order of 15 to 60 degrees/sec². When the maximum angular speed (slewing rate) is achieved, speed is held more or less constant until, as the desired engine deflection position is reached, deceleration occurs. Normal overshoot results in a typically damped sinusoidal oscillation as the engine position--and hence the side-force--"settles down" on the selected value.

Secondary Injection - Upon command, one of two uni-directional (that is, plus or minus) valve actuators is opened to the set-point corresponding to the required secondary flow to the nozzle. Since these actuators are many times smaller than those required for gimbaling and have no significant inertia load, the peak acceleration and velocities are many times higher. Once the valve port is opened, secondary flow follows almost instantaneously and establishes the nozzle flow pattern for side-force generation. The latter being strictly a supersonic flow phenomenon, time lags of the order found in mechanical systems are non-existent.

It can be surmised that, relatively speaking, for large engines the response possible from secondary injection means can be much higher (if advantageous) than the response from gimbaling means. This comparison is represented in FIG 18:

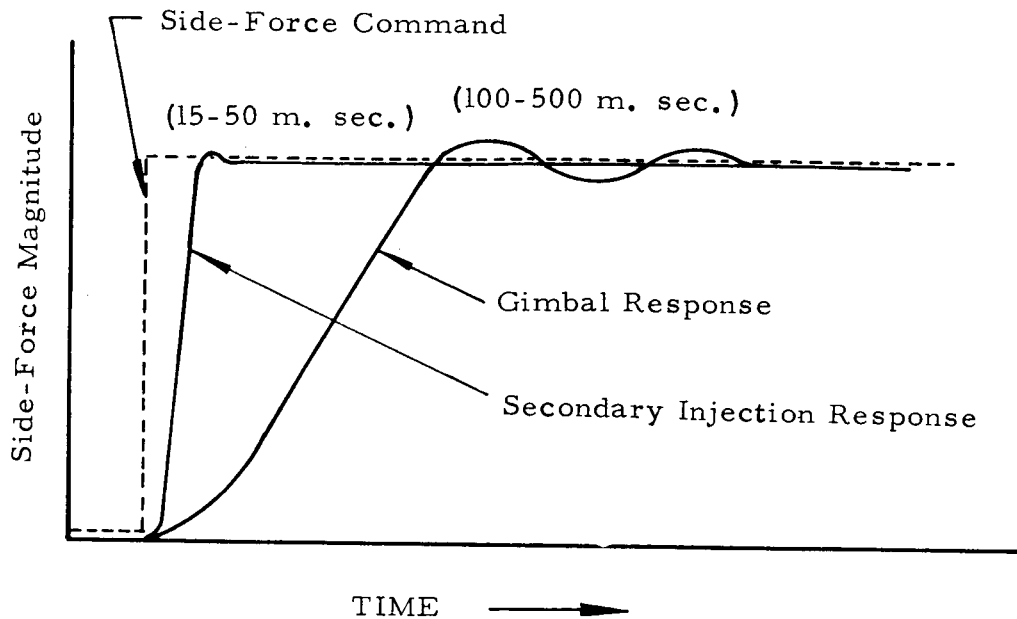


FIGURE 18. COMPARATIVE SIDE-FORCE RESPONSE

Since high side-force response is ultimately available from secondary injection devices, a digital control mode is probably quite feasible, in contrast to the proportional (analog) side-force generation scheme discussed above. A digital side-force system in its simplest form would be a conventional on-off system. Either pulse frequency or pulse-width variation--or a combination of the two--could provide the total side impulse required. One strong advantage for digital-mode side-force generation is the resulting simplification of the injectant valve/actuator combination in going from a proportional-flow (throttling) device to an on-off device. One of the injection schemes noted earlier (FIG 12b) employs a multiple bi-stable valve arrangement. It would be therefore, an example of a digitally operated side-force system.

4. Overall Performance

1. Performance--ultimately payload performance--is determined by two well known vehicle characteristics: Powerplant specific

impulse and vehicle mass ratio. In comparing the relative performance potential of gimbaling and secondary injection these two factors (I_{sp} , λ) must be viewed concurrently with comparison of the rocket engine configurations. The following analysis, though simplified and qualitative, reflects trends in the comparative performance of powerplants using the gimbaling and secondary injection engine side-force generation methods. It is based on the fairly reasonable assumption that specific impulse and--to a somewhat lesser extent--engine hardware weight are affected in such a way as to lower performance as the thrust-vector deflection angle operating point is increased.

Specific Impulse

The specific impulse comparison goes as follows (FIG 19a). The two rocket engine configurations will develop essentially the same I_{sp} at a zero thrust-vector deflection angle condition if the nozzle expansion area ratios are the same. It is quite possible that because of thrust-chamber interference and vehicle envelope limitations, the gimballed configuration may become area-ratio limited and, the fixed nozzle of the secondary injection configuration can be permitted to have a higher expansion area ratio. In such a case the secondary injection configuration performance would of course be higher at the zero deflection angle. This advantage is not shown in the figure, however.

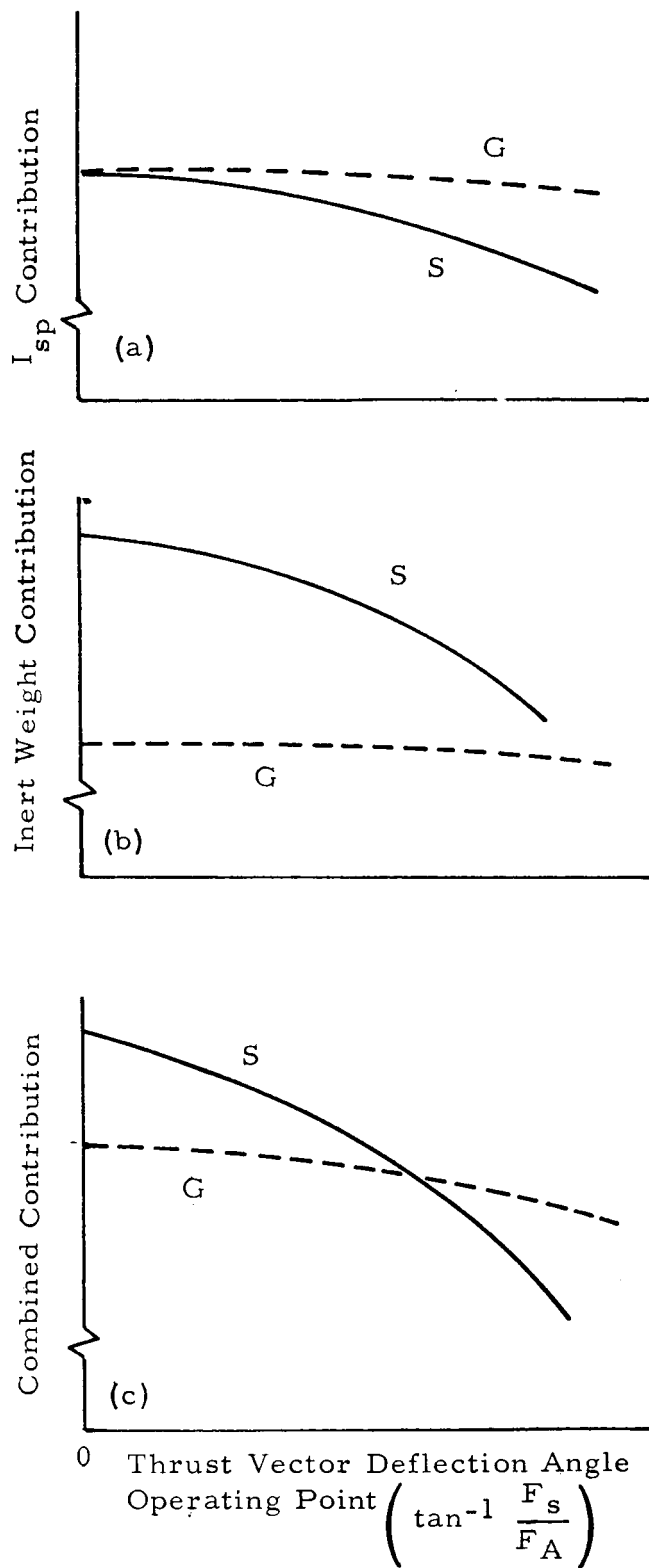
As the deflection angle maximum operating point is increased, the effective I_{sp} of the gimballed engine falls off--but rather slightly--because of the $1-\cos$ characteristic (by way of example, at a 6° deflection, I_{sp} losses are .548 percent).

The magnitude of the losses in the secondary injection case are not so clearcut and they will certainly be different for each configuration. Here, an estimate of effective I_{sp} must relate both the primary (Combustion chamber) propellant flow and the secondary injectant flow to the axial thrust, or

$$I_{sp}^{Eff} = \frac{F_{ax}}{W_{prim} + W_{sec}}$$

As discussed in the earlier analytical section of this report, the secondary propellant flow can contribute significantly to axial thrust, the amount of this contribution being a function of the secondary injection

INDEX OF OVERALL VEHICLE PAYLOAD PERFORMANCE



MTP-P&VE-P-62-10

FIGURE 19. RELATIVE PAYLOAD PERFORMANCE ASPECTS
OF GIMBALING AND SECONDARY INSPECTION VS THRUST
VECTOR DEFLECTION OPERATING POINT

angle and nozzle station (FIG 9, lower plot). To remain conservative, this contribution should perhaps be assumed to be zero, as it might be for extreme angles of counterstream injection. Performance thus falls off at a considerably higher rate than for the gimbaling case as a result of increasing secondary flow required for the increasing deflection angle. The importance of achieving a high side-specific-impulse becomes quite clear, since this overall powerplant performance loss is tied directly to the configuration's side-force performance. It should be noted that side-specific impulse tends to drop off somewhat with increasing injectant flow rates. This point was made earlier in the discussion of the secondary injection flow phenomenon. This tendency is shown by the non-linearity of the upper curve in FIG 6.

Note that the better effectiveness of secondary injection configurations from the standpoint of point-of-application as discussed in this section has not been brought into the above consideration.

Mass Ratio

As discussed earlier, a vehicle with a gimbaled engine is expected to have significantly higher structural inert weight than an equivalent vehicle with a fixed engine (as with secondary injection). The amount of weight saving depends on the degree to which advantage is taken of the fixed engine situation by the type of thrust chamber mounting, the amount of engine repackaging allowed, etc. This last point is discussed in conjunction with the earlier sample NOVA vehicle examples of this report. Therefore, at the zero deflection operating point, the secondary injection configuration should have a significantly lower vehicle weight than its gimbaled engine equivalent; see FIG 19b.

At finite deflection-angle operating-points some slight weight increases might be expected. Here the gimbaled engine should be fairly insensitive; the major weight penalty is initially taken largely to acquire the capability of gimbaling, regardless of the deflection-operating-point determined subsequently. On the other hand, the equipment to achieve secondary injection will be sized for a nominal operating point; its weight will increase somewhat with the deflection requirement. These trends are reflected in the curve.

Overall Payload Performance

Figure 19C attempts to show the combined effect of specific impulse and inert weight (mass ratio) variation with the thrust-vector deflection-operating-point. Note that a crossover situation exists at some operating point: secondary injection yields superior performance for lower deflections, gimbaling yields superior performance for higher deflections. The crux of the question of gimbaling versus secondary injection is likely reached in the determination of the absolute quantities for the ordinate and abscissa for the curves of FIG 19C. The order of pay-off of shifting to secondary injection would then be clear.

A fact that considerably complicates the comparison suggested above is that the critical parameter, the thrust-vector deflection-operating-point, is notably variable for each vehicle and for each stage of the same vehicle. Also, values for this operating point are established on the basis of probability. That is, a prediction has no unique value for any given vehicle stage at any given point in its flight program. Finally, the questions of engine-out capability, thrust-chamber cant angle, and vehicle c.g. travel during the burning period must all be brought into any study which addresses the applicability of secondary-injection side-force systems to a particular vehicle.

RESULTS AND CONCLUSIONS

1. The gaseous secondary injection flow phenomenon is under wide investigation. Due largely to the complexity of the nozzle flow field, a purely analytical treatment of the problem is not feasible at this time. A theory which shows fairly good agreement with experiment is, however, available.

2. Hydrogen-fueled rocket engines are especially well-suited to the use of secondary-injection side-force generation. This is because hydrogen alone, or as the primary component of the combustion product, is an efficient injectant. Hence, there is no requirement for fluids not already available in the engine.

3. The specific impulse developed by gimbaled and secondary injection versions of a hydrogen-fueled engine differ substantially only during the time large side-forces are being generated. (Those equivalent to 4 or 5 degrees of equivalent gimbaling.) Under these conditions the secondary injection version may fall behind the gimbaled version by as much as 1 or 2 percent. But, in an actual vehicle application with a lesser mean side-force requirement there will likely be no substantial difference in performance. The above does not consider the performance improvement possible via an increased nozzle expansion area ratio within a vehicle diametral limitation. The fixed thrust-chamber with secondary-injection, permits such an increase over an equivalent gimbaling configuration.

4. Side-force generation via secondary fluid injection permits a fixed, as opposed to a gimbaled, engine installation. From the vehicle standpoint, this fact should significantly enhance performance and reliability. It will also tend to simplify the powerplant engineering problem in general. Vehicle inert weight may be significantly reduced.

5. The equipment chosen for secondary injection must be viewed as a distinct subsystem of the engine. This is because it is a vital part of the engine fluid-flow circuit. Hence it must follow the same strictly controlled development and qualification program as do the other engine subsystems, e. g. turbopump, thrust-chamber, and engine controls.

6. Of the several specific injection approaches suggested so far (viz., heated hydrogen alone, combustion-chamber tap, utilization of turbine exhaust, and auxiliary combustion devices), many are present state-of-the-art "hardware-level" engineering developments and lend themselves readily to engine-system integration. It is, in fact, in this area that effort must now be concentrated.

RECOMMENDATION

The purpose of this report has been to point-up the present practicability and need for an engineering-level development effort to generate an integrated secondary injection side-force capability in our hydrogen engine programs. We feel that the available background--analytical and experimental--validates this conclusion. Culminating in the present NASA-contracted United Aircraft Corporation Research Laboratories effort (NAS8-5070) investigation to date has produced the requisite information in depth to allow hardware-level engineering to commence immediately. The few potential problem areas and unanswered questions relating to performance which remain are closely tied to such hardware developments. We therefore recommend that development--appropriately linked to program requirements--be initiated promptly.

APPENDIX I

STATEMENT OF WORK FOR CONTRACT NAS8-5070

TITLE: The Use of Hydrogen as a Secondary Injectant for Thrust Vector Control

OBJECTIVE: To investigate the use of heated hydrogen, or combustion products of hydrogen and oxygen, as a secondary injectant fluid.

The project shall lead to design information that is required for effective use of heated hydrogen, or combustion products of hydrogen and oxygen as a secondary injectant in any nozzle (conventional or unconventional, including APG)*. The design information shall be verified by conducting suitable experiments in sub-scale and (if feasible) representative full-scale nozzles.

TASK 1.

Existing data and design information regarding the use of secondary injectants shall be utilized to the greatest extent possible. The necessary correlating parameters to enable various low molecular weight gases to be fitted into the existing design criteria shall be developed as required. Suitable scaling laws, considering geometrical influence of nozzle configurations shall also be developed, if needed, in order that the design data will be universally applicable. Suitable cold and hot flow model experiments shall be conducted, as required, to enable analytical models to be established from which correlations can be developed.

TASK 2.

Additional cold and hot flow tests shall be conducted on appropriately scaled nozzles (at whatever size is necessary and sufficient) to verify the correlation and design information. Performance predictions shall also be verified. These latter tests should be conducted using direct force measurements rather than integration of pressure fields.

*Adverse Pressure Gradient

APPENDIX II

ANALYSIS OF THE EXPRESSION FOR SIDE-FORCE

Beginning with equation 3, the following breakout may be made:

$$\frac{F_2}{F_1} = \left[\frac{Cf \left(\frac{V_2}{a^*_2} \sin \alpha + 0.9 \right) + \left(1 + \frac{1}{\gamma M_2^2} \right) \frac{V_2}{a^*_2} \cos \alpha}{V_1/a^*_1} \right] \frac{a^*_2}{a^*_1} \frac{\dot{W}_2}{\dot{W}_1}$$

$$\frac{F_2}{F_1} = \left[\frac{Cf \left(V_2 \sin \alpha + 0.9 a^*_2 \right) + \left(1 + \frac{1}{\gamma M_2^2} \right) V_2 \cos \alpha}{V_1} \right] \frac{\dot{W}_2}{\dot{W}_1} \quad (A-1)$$

$$\frac{F_2}{F_1} = \left[Cf \left(\sin \alpha + 0.9 \frac{a^*_2}{V_2} \right) + \left(1 + \frac{1}{\gamma M_2^2} \right) \cos \alpha \right] \frac{V_2}{V_1} \frac{\dot{W}_2}{\dot{W}_1} \quad (A-2)$$

$$\frac{F_2}{F_1} = \left[Cf \left(\overbrace{\sin \alpha + 0.9/M^*_2}^{\phi_i} + \overbrace{\left(1 + \frac{1}{\gamma M_2^2} \right) \cos \alpha}^{\phi_r} \right) \right] \frac{V_2}{V_1} \frac{\dot{W}_2}{\dot{W}_1} \quad (A-3)$$

Where ϕ_i = Induced Term, sec^2/ft .

ϕ_r = Reaction Term, sec^2/ft .

REACTION TERM

The reaction thrust term, ϕ_r , may be derived as follows:

The conventional expression for reaction thrust may be written

$$F = \frac{\dot{W}}{g} V_e + (P_e - P_a) A_e \quad (A-4)$$

The reaction thrust term of equation (A-3) may be equated to give the following:

$$\frac{\dot{W}}{g} V_e + (P_e - P_a) A_e = \left(1 + \frac{1}{\gamma M_2^2}\right) \cos \alpha \frac{\dot{W}}{g} V_2 \quad (\text{A-5})$$

or

$$\frac{\dot{W}}{g} V_e + (P_e - P_a) A_e = \frac{\dot{W}}{g} V_2 + \frac{\dot{W}}{\gamma g} \frac{V_2}{M_2^2} \quad (\text{A-6})$$

The directional correction $\cos \alpha$ has been dropped for clarification purposes.

Dropping the equivalent momentum term

$$(P_e - P_a) A_e = \frac{\dot{W}_e V_e}{\gamma M_2^2 g} \quad (\text{A-7})$$

The following identities may be written:

$$\dot{W}_2 = \rho_e V_e A_e \quad (\text{A-8})$$

$$M_2^2 = \frac{V_2^2}{\frac{A_e^2}{A_e}} \quad (\text{A-9})$$

$$a_e^2 = \frac{\gamma g P_2}{\rho_2} \quad (\text{A-10})$$

Substituting (A-8), (A-9) and (A-10) into (A-7) we get:

$$(P_e - P_a) A_e = \rho_2 A_2 V_2 \cdot \frac{1_2}{V_2} \frac{\gamma g P_2}{\rho_2} \frac{V_2}{\gamma g} = P_2 A_2 \quad (\text{A-11})$$

or

$$(P_e - P_a) A_e = P_2 A_2 \quad (\text{A-12})$$

The ambient pressure P_a is assumed to be equal to zero for purposes of this analysis.

$$\therefore P_e A_e = P_2 A_2 \quad (A-13)$$

INDUCED TERM

As has been shown before, the induced term ϕ_i is a function of momentum change. Referring again to FIG 5, it is fairly apparent that the momentum change of injected fluid may be written

$$\Delta \text{momentum} = V_2 \dot{W}_2 \sin \alpha + V_2 \dot{W}_2 \cos \theta \quad (A-14)$$

This may be equated to the induced portion of equation (A-3), giving

$$\Delta \text{momentum} = \left(\sin \alpha + \frac{0.9}{M_2^*} \right) V_2 \dot{W}_2 = V_2 \dot{W}_2 \sin \alpha + V_2 \dot{W}_2 \cos \theta \quad (A-15)$$

$$\therefore \frac{0.9}{M_2^*} V_2 \dot{W}_2 = V_2 \dot{W}_2 \cos \theta \quad (A-16)$$

$$\frac{0.9}{M_2^*} V_2 = V_2 \cos \theta$$

$$\text{using } M_2 = \frac{V_2}{a_2^*}$$

$$\text{we get } 0.9 a_2^* = V_2 \cos \theta$$

The number 0.9 is empirical: determined from experimental results.

CORRELATION WITH EXPERIMENTAL DATA

Restating equation 4 (Body of the Report):

$$\frac{F_2}{F_1} = \frac{\left[\frac{Cf}{f_{2-D}} \times f_{2-D} \left(\frac{V_2}{a^*_2} \sin \alpha + 0.9 \right) + \left(1 + \frac{1}{\gamma M_2} \right) \frac{W_2}{a^*_2} \cos \alpha \right] \frac{a^*_2}{a^*_1} \frac{W_2}{W_1}}{V_1 / a^*_1}$$

A sample calculation may now be made for the following two cases selected from the referenced figures of this report. (It is to be kept in mind that these figures represent experimental data.) The fluid is air at ambient temperature for both the primary and secondary conditions.

	<u>Case I</u>	<u>Case II</u>	<u>Reference Fig. No.</u>
M_2	1.0	1.0	
α	40	30	Fig. 9
$\frac{Cf}{f_{2-D}}$	0.80	0.60	Fig. 9
f_{2-D}			
f_{2-D}	2.95	2.95	
M_1	4.13	4.13	
$\frac{W_2}{W_1}$	0.01	0.05	

Assume: $a^*_1 = a^*_2$ (like on like injection). V/a^* is tabulated as a function of Mach Number in NACA TR 1135.**

Making the substitutions: (Case I)

$$\frac{F_2}{F_1} = \left[0.80 (2.95) (.643 + 0.9) + \left(1 + \frac{.766}{1.4} \right) \right] \frac{0.01}{2.154}$$

$$\frac{F_2}{F_1} = 0.023 \text{ or } \frac{F_2/F_1}{\frac{W_2}{W_1}} = 2.3$$

**Equations, Tables, and Charts for Compressible Flow, NASA Report 1135, dated 1953.

As can be seen the results of these calculations correlate with the experimental data shown in FIG 9.

$$\frac{F_2}{F_1} = \left[0.60 (2.95) (0.5 + 0.9) + \left(1 + \frac{0.866}{1.4} \right) \right] \frac{0.05}{2.154}$$

$$\frac{F_2}{F_1} = 0.092 \text{ and } \frac{F_2 F_1}{W_2 W_1} = 1.84$$

APPENDIX III

PERFORMANCE COMPARISON OF GIMBALED
AND SECONDARY INJECTION VERSIONS OF A MODEL STAGE

Two similar Nova-class stage designs employing two M-1 engines were compared in performance. One version had gimballed engines and the other employed secondary injection side-force generation. These are shown schematically in FIG 14. The low center of gravity position is typical for a squat (low L/D) hydrogen-oxygen stage in which the liquid oxygen tank is aft and the hydrogen tank forward.

The basis for this stage layout was the conceptual studies of Nova vehicles conducted by the Advanced Flight Systems Branch, Propulsion and Vehicle Engineering Division circa June 1962. The vehicle chosen as a model here employed the following engine complement in its three stages, respectively: 10 F-1's, 2 M-1's, and 1 J-2.

A determination was desired as to the effect on the axial specific impulse developed by the two versions as the powerplant operated over the side-force range. Specifically, this information was to be presented in two curves (one for each version) which plotted I_{sp} versus effective gimbal angle. Such a plot is simple for the gimballed case; the axial specific impulse at zero gimbal angle is diminished by the factor $1 - \cos \delta$, where δ is the gimbal deflection. The performance of the secondary injection case is considerably more complex, as will be shown.

The following assumptions and limitations apply:

1. The engine exit-plane to vehicle c.g. distances are the same for the two cases, and the nozzle expansion area ratios are identical ($\epsilon = 40$).
2. Secondary injection is performed using the turbopump exhaust gases as the injectant; the mechanism for accomplishing this is not discussed.

3. The overall performance of the M-1 with a 40:1 expansion area ratio was taken to be 435 seconds*. This value is used as a baseline for the zero side-force condition thrust.

4. The M-1 thrust chamber and turbopump exhaust flow parameters were assumed to have the following characteristics (based on consultation with personnel at Aerojet-General):

Main Thrust Chamber Gas

a. Flow Rate (maximum)	2728.5 lb/sec
b. Temperature (stagnation)	6152.4 °R
c. Average Molecular Weight	13.1
d. Ratio of Specific Heats (γ)	1.257
e. Axial Thrust (does not include turbine exhaust thrust)	1,200,000 lb

Turbine Exhaust Gas

a. Flow Rate (maximum)	97.6 lb/sec (3.6% of total engine flow rate)
b. Temperature (stagnation)	1511 °R
c. Average Molecular Weight	3.62
d. Ratio of Specific Heats (γ)	1.362
e. Axial Thrust Derived from total turbine exhaust flowing through nozzles (expansion area ratio ≈ 2 in the present design weight results in $I_{spTE} = 299$ sec)	29,150 lb

The following calculations were made to derive the data presented in FIG 15, a plot of effective powerplant specific impulse versus effective thrust vector deflection angle. Again, these data are specifically for the model stage configuration depicted in FIG 14. Calculations were made on the basis of analytical expressions developed in the section of this report entitled, "The Gaseous Secondary Injection Flow Phenomenon."

*This value is not that officially specified for the M-1 engine.

SECONDARY INJECTION VERSION

1. Amplification Factor

On the basis of analytical and experimental work generally surveyed, the following air-on-air amplification values (K_1) have been assumed:

$$2.9 \text{ @ } 1\% - \text{secondary flow rate ratio, } \left(\frac{\dot{W}_2}{\dot{W}_1} \right)$$

$$2.5 \text{ @ } 3.6\%^* - \text{secondary flow rate ratio } \left(\frac{\dot{W}_2}{\dot{W}_1} \right)$$

These values are then corrected for the M-1 engine using turbine exhaust as the injectant. The correlation term is developed as follows:

$$K_2 = K_1 \sqrt{\frac{M_1}{M_2} \times \frac{T_{T_2}}{T_{T_1}}}$$

$$K_2 = K_1 \sqrt{\frac{13.1}{3.62} \times \frac{1511}{6152}}$$

$$K_2 = K_1 \sqrt{0.889} = 0.943 K_1$$

Hence, the corrected amplification factors are:

$$\begin{array}{ll} 0.943 \times 2.9 = 2.73 & \text{at } 1\% \text{ secondary flow} \\ 0.943 \times 2.5 = 2.36 & \text{at } 3.6\% \text{ secondary flow} \end{array}$$

*Maximum available turbine exhaust flowrate

2. Side-Force Magnitudes

Employing the curve shown here of amplification factor (corrected) versus flow rate ratio (FIG 20), the side specific impulse and side-force magnitudes may be calculated. Four flow rate ratio points are used, viz. 1, 2, 3, and 3.6%.

$$I_{sp}(\text{side}) = I_{sp}(\text{axial}) \times K_2$$

For	1%	$I_{sp}(\text{side}) = 435 \times 2.73 = 1188 \text{ sec}$
	2%	$= 435 \times 2.58 = 1122 \text{ sec}$
	3%	$= 435 \times 2.47 = 1074 \text{ sec}$
	3.6%	$= 435 \times 2.36 = 1027 \text{ sec}$

$$F(\text{side}) = I_{sp}(\text{side}) \times \dot{W}_2$$

For	1%	$F(\text{side}) = 1188 \times 27.29 = 32.4 \times 10^3 \text{ lb}$
	2%	$= 1122 \times 54.57 = 61.2 \times 10^3 \text{ lb}$
	3%	$= 1074 \times 81.86 = 87.9 \times 10^3 \text{ lb}$
	3.6%	$= 1027 \times 97.6 = 100.2 \times 10^3 \text{ lb}$

3. Equivalent Gimbal Deflection

Using the side-force values developed above and the stage geometry shown in FIG 14, moments about the center of gravity and thence equivalent gimbal deflections (the gimbaled version is here the reference) can be derived. It should be noted that the longer effective moment arm of the secondary injection version, over the gimbaled version, offers a considerable advantage here (see FIG 17). Note also that the equivalent gimbal angle is significantly higher for the stage at engine start-up (lower center of gravity point) as compared with the final engine-cutoff condition. The moments for the startup and cutoff conditions are:

(Startup Case)

$$M_{1\%} = 32.4 \times 10 \times 66.67 = 2.16 \times 10^6 \text{ ft-lb}$$

$$M_{2\%} = 61.2 \times 10 \times 66.67 = 4.08 \times 10^6 \text{ ft-lb}$$

$$M_{3\%} = 87.9 \times 10 \times 66.67 = 5.86 \times 10^6 \text{ ft-lb}$$

$$M_{3.6\%} = 100.2 \times 10 \times 66.67 = 6.68 \times 10^6 \text{ ft-lb}$$

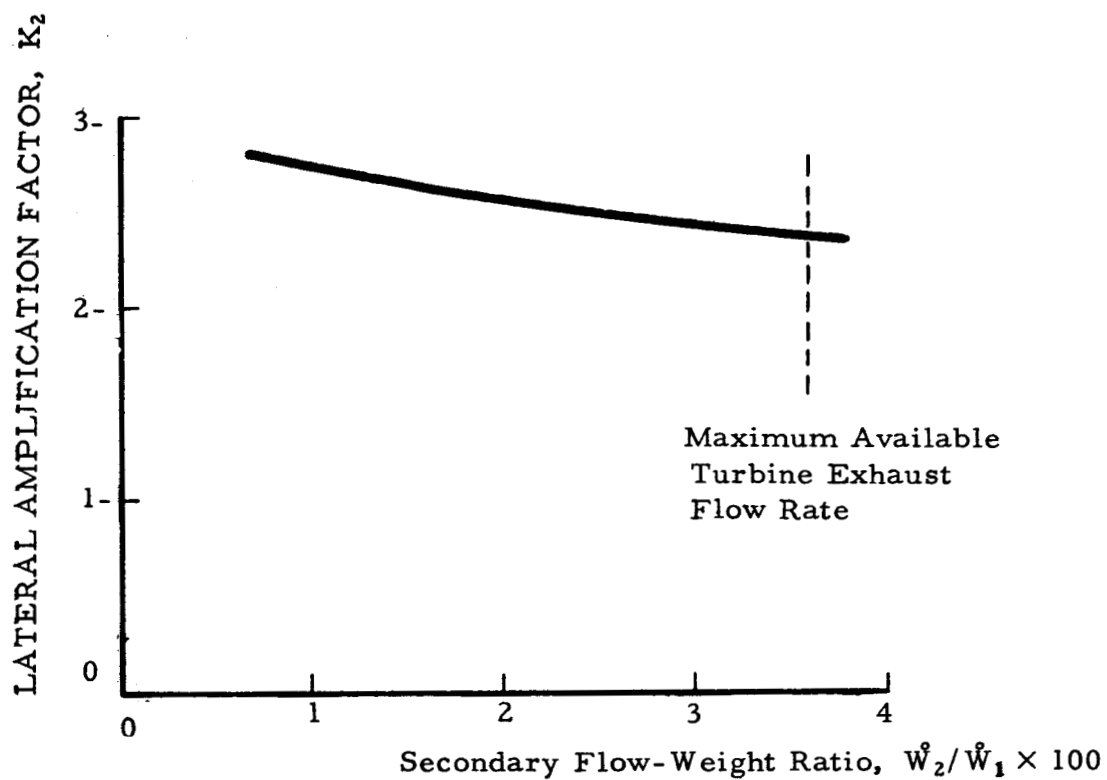


FIGURE 20. LATERAL AMPLIFICATION FACTOR VERSUS SECONDARY FLOW-WEIGHT RATIO FOR THE M-1 USING TURBINE EXHAUST SECONDARY INJECTION

MTP-P&VE-P-62-10

(Cutoff Case)

$$M_{1\%} = 32.4 \times 10 \times 118.9 = 3.85 \times 10^6 \text{ ft-lb}$$

$$M_{2\%} = 61.2 \times 10 \times 118.9 = 7.28 \times 10^6 \text{ ft-lb}$$

$$M_{3\%} = 87.9 \times 10 \times 118.9 = 10.46 \times 10^6 \text{ ft-lb}$$

$$M_{3.6\%} = 100.2 \times 10 \times 118.9 = 11.92 \times 10^6 \text{ ft-lb}$$

The equivalent gimbal angle is the deflection of a gimballed engine (FIG 14) producing the moments derived above; Hence:

$$\delta = \sin^{-1} \frac{M_s}{FAX \cdot LGIM}$$

(Startup Case)

$$\delta_{1\%} = \sin^{-1} \frac{2.16 \times 10^6}{1.229 \times 10^6 \times 44.2}$$

$$= \sin^{-1} .0398 = 2^\circ 17', \text{ or } 2.28^\circ$$

$$\delta_{2\%} = \sin^{-1} \frac{4.08 \times 10^6}{1.229 \times 10^6 \times 44.2}$$

$$= \sin^{-1} .0752 = 4^\circ 19', \text{ or } 4.32^\circ$$

$$\delta_{3\%} = \sin^{-1} \frac{5.86 \times 10^6}{1.229 \times 10^6 \times 44.2}$$

$$= \sin^{-1} .108 = 6^\circ 12', \text{ or } 6.20^\circ$$

$$\delta_{3.6\%} = \sin^{-1} \frac{6.68 \times 10^6}{1.229 \times 10^6 \times 44.2}$$

$$= \sin^{-1} .123 = 7^\circ 4', \text{ or } 7.07^\circ$$

(Cutoff Case)

$$\begin{aligned}\delta_{1\%} &= \sin^{-1} \frac{3.85 \times 10^6}{1.229 \times 10^6 \times 118.9} \\ &= \sin^{-1} .0264 = 1^\circ 31', \text{ or } 1.52^\circ\end{aligned}$$

$$\begin{aligned}\delta_{2\%} &= \sin^{-1} \frac{7.28 \times 10^6}{1.229 \times 10^6 \times 118.9} \\ &= \sin^{-1} .0498 = 2^\circ 52', \text{ or } 2.87^\circ\end{aligned}$$

$$\begin{aligned}\delta_{3\%} &= \sin^{-1} \frac{10.46 \times 10^6}{1.229 \times 10^6 \times 118.9} \\ &= \sin^{-1} .0716 = 4^\circ 6', \text{ or } 4.10^\circ\end{aligned}$$

$$\begin{aligned}\delta_{3.6\%} &= \sin^{-1} \frac{11.92 \times 10^6}{1.229 \times 10^6 \times 118.9} \\ &= \sin^{-1} .0815 = 4^\circ 41', \text{ or } 4.68^\circ\end{aligned}$$

Summarizing the effective gimbale angle information for the eight cases, the following tabulation is given:

Secondary Flow-Rate Ratio	Startup Case	Cutoff Case
1%	2.28°	1.52°
2%	4.32°	2.87°
3%	6.20°	4.10°
3.6%	7.07°	4.68°

4. Axial Specific Impulse Reduction Due to Secondary Injection

The axial specific impulse during side-force generation in the secondary injection version will be affected by two actions:

a. The loss of axial thrust and impulse (from the small turbine exhaust nozzle), since some or all of this flow is routed through the secondary injectant nozzles during side-force generation.

b. The gain of specific impulse from the axial specific impulse contribution of the secondary injectant. This gain will normally be of the same order or less than the loss cited above. The axial thrust loss is assumed to be a linear function of the amount of flow routed away from the axial nozzles. Hence, for the calculated flow rate points, the thrust which is lost is given by the following tabulation:

Secondary Flow-Weight Ratio	Axial Thrust Loss (lb)
1%	8.10×10^3
2%	16.2×10^3
3%	24.3×10^3
3.6%	29.2×10^3

The axial contribution of the secondary injectant flow is assumed to be 200, 100, 50, and 35 seconds for the four points (FIG 21). The thrust added is simply:

$$F_{AX} = \dot{W}_2 \times I_{spAX}$$

$$\Delta F_{AX1\%} = 27.29 \times 200 = 5.46 \times 10^3 \text{ lb}$$

$$\Delta F_{AX2\%} = 54.57 \times 100 = 5.46 \times 10^3 \text{ lb}$$

$$\Delta F_{AX3\%} = 81.86 \times 50 = 4.09 \times 10^3 \text{ lb}$$

$$\Delta F_{AX3.6\%} = 97.6 \times 35 = 3.42 \times 10^3 \text{ lb}$$

The net axial thrust resulting from this respective loss and gain is negative, i. e. a thrust reduction of:

$$F_{AX1\%} = (1,291.5 - 8.10 + 5.46) \times 10^3 = 1,288.9 \times 10^3 \text{ lb}$$

$$F_{AX2\%} = (1,291.5 - 16.2 + 5.46) \times 10^3 = 1,280.8 \times 10^3 \text{ lb}$$

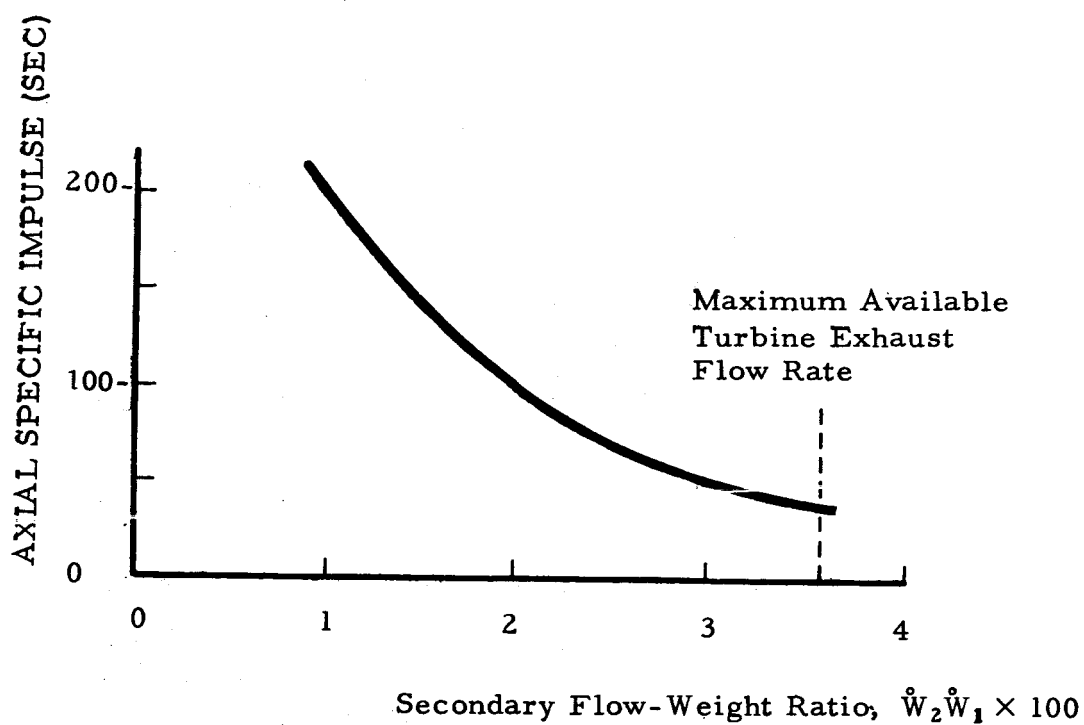


FIGURE 21. AXIAL SPECIFIC IMPULSE CONTRIBUTION OF SECONDARY INJECTANT VERSUS SECONDARY FLOW-WEIGHT RATIO

$$F_{AX_{3\%}} = (1,291.5 - 24.3 + 4.09) \times 10^3 = 1,271.3 \times 10^3 \text{ lb}$$

$$F_{AX_{3.6\%}} = (1,291.5 - 29.2 + 3.42) \times 10^3 = 1,265.7 \times 10^3 \text{ lb}$$

The reduction in specific impulse is determined by ratioing the above thrust values with that of the engine in the zero side-force condition, vis. 1,291,500 lb.

Secondary Flow-Weight Ratio	$\frac{I_{sp}}{I_{sp(nom)}}$	$I_{sp(sec)}$	$\Delta I_{sp(sec)}$
0	1.0000	435.0	0
1%	.9980	434.1	-0.9
2%	.9917	431.4	-3.6
3%	.9844	423.2	-6.8
3.6%	.9800	426.3	-8.7

5. Axial Specific Impulse Reduction Due to Gimbaling

The impulse reduction experienced in gimbaling is simply the cosine loss for the given deflection angle:

Gimbal Deflection	$\cos \delta$, or $\frac{I_{sp}}{I_{sp(nom)}}$	$1 - \frac{I_{sp}}{I_{sp(nom)}} \times 100$
0	1.00000	0.000
1	.99985	.015
2	.99939	.061
3	.99863	.137
4	.99756	.244
5	.99619	.381
6	.99452	.548
7	.99255	.745
8	.99027	.973

6. Plot of Engine Specific Impulse Versus Effective Gimbal Angle

The correlation of secondary flow-weight ratio with equivalent gimbal angle (secondary injection case) for the startup and shutdown cases was presented on page 69. Engine specific impulse for various secondary flow-weight ratios is given in 4 above (page 72).

A tabulation showing the specific impulse reduction with increasing gimbal angle (gimbaled engines) is on page 72.

These data are presented as FIG 15 in the body of the report.

REFERENCES

1. Erickson, L. H., and Bell, Jr., H. S., Optimum Design Investigation - Thrust Vector Control System, AFSC-TR-61-1, Thiokol Chemical Corp., March 1962.
2. Chamay, A. J., and Sederquist, R. A., An Experimental Investigation of Shock Vector Control with Gaseous Secondary Injection, ARS Paper 2216-61 (1961).
3. Hausmann, G. F., Thrust Axis Control of Supersonic Nozzles by Airjet Shock Control. U. A. C. Research Laboratories Report R-63143-24, May 1952.
4. Lingen, A., Jet-Induced Thrust-Vector Control Applied to Nozzles Having Large Expansion Ratios. U. A. C. Research Laboratories Report R-0937-33, March 1957.
5. Olsen, R. E. and Burr, J. W: Exploratory Tests of Jet-Induced Thrust-Vector Control by Injection Through a Slot at the Nozzle Exit. U. A. C. Research Laboratories Report UAR-0886, April 1961.
6. Rodriguez, C. J., An Experimental Investigation of Jet-Induced Thrust Vector Control Methods. Bulletin of the 17th Meeting JANAF-ARPA-NASA Solid Propellant Group, May 1961, Vol. 3 September 1961, CONFIDENTIAL.
7. Chapman, D. R., Knehn, D. M., and Larson, H. K.: Investigation of Separated Flows in Supersonic and Subsonic Streams with Emphasis on the Effort of Transition. National Advisory Committee for Aeronautics, Technical Note 3869, March, 1957.
8. Hausmann, G. F.: Investigation of the Use of Hydrogen as a Secondary Injectant for Thrust Vector Control (Proposal), U. A. C. Research Laboratories Report N. A. R. -P-A21, May, 1962.

APPROVAL

MTP-P&VE-P-62-10

ENGINE-INTEGRATED SECONDARY INJECTION SIDE-FORCE
GENERATION FOR THE HYDROGEN-FUELED ROCKET ENGINE

By William J. D. Escher and Donald D. Thompson

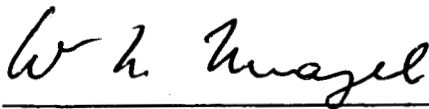
The information in this report has been reviewed for security classification. Review of any information concerning Department of Defense or Atomic Energy Commission programs has been made by the MSFC Security Classification Officer. This report, in its entirety, has been determined to be unclassified.



for J. THOMSON
Chief, Advanced Propulsion Section



H.G. PAUL
Chief, Propulsion and Mechanics Branch



W. A. MRAZEK
Director, Propulsion and Vehicle Engineering Division

DISTRIBUTION

M-DIR	Dr. von Braun
M-DEP-R&D	Dr. Rees
M-AERO-DIR	Dr. Geissler
M-AERO-TS	Mr. Murphree
M-AERO-A	Mr. Linsley
M-AERO-D	Mr. Baker
M-ASTR-DIR	Dr. Haeussermann
M-ASTR-TSA	Mr. Daussman
M-ASTR-R	Mr. Taylor
M-ASTR-N	Mr. Moore
M-COMP-DIR	Dr. Hoelzer
M-COMP-S	Mr. Shaver
M-FPO-DIR	Mr. Koelle
M-FPO	Mr. Williams
M-FPO	Mr. Sanders
M-FPO	Mr. Spears
M-ME-DIR	Mr. Kuers
M-HME-P	Mr. Knox
M-HME-I	Mr. Burns
M-P&VE-DIR	Dr. Mrazek
	Mr. Weidner
	Mr. Hellebrand
M-P&VE-TSN	Mr. Finzel
M-P&VE-REL	Mr. Burrows
M-P&VE-O	Mr. Belew
M-P&VE-N	Col. Fellows
M-P&VE-V	Mr. Palaoro
M-P&VE-F	Mr. Goerner
	Mr. Barker
M-P&VE-FM	Mr. Jordan
M-P&VE-FS	Mr. Pedigo
	Mr. Johns
M-P&VE-E	Mr. Schulze
M-P&VE-E	Mr. Jacobi
M-P&VE-S	Mr. Kroll
M-P&VE-SA	Mr. Blumrich
M-P&VE-P	Mr. Paul
	Mr. McCool
	Mr. Isbell

DISTRIBUTION (CONTINUED)

M-P&VE-PA	Mr. Thomson
	Mr. Chandler
	Mr. Lombardo
	Mr. Thompson
M-P&VE-PE	Mr. Bergeler
M-P&VE-PH	Mr. Connell
M-P&VE-PI	Mr. Voss
M-P&VE-PL	Mr. Reed
M-P&VE-PM	Mr. Fuhrmann
M-P&VE-PP	Mr. Heusinger
M-P&VE-PS	Mr. Eilerman
M-P&VE-PT	Mr. Wood
M-P&VE-M	Dr. Lucas
M-P&VE-ADMP	Mr. Hofues
M-QUAL-DIR	Mr. Grau
M-QUAL-M	Mr. Urbanski
M-RP-DIR	Dr. Stuhlinger
M-RP-R	Mr. Miles
M-REL	Mr. Peigler
M-SAT	Mr. Dannenberg
M-TEST-DIR	Mr. Heimburg
M-TEST-C	Mr. Haukohl
M-MS-H	Mr. Akens
M-MS-IP	Mr. Remer
M-MS-IPL (8)	

Scientific & Technical Information Facility

Attn: NASA Representatives

(S-AK/RKT)

P. O. Box 5700

Bethesda, Maryland

NASA Headquarters:

Code RP	Mr. Sloop
	Mr. Burlage

Code MLV	Dr. Hall
	Mr. Lovejoy

DISTRIBUTION (CONCLUDED)

Code MLP Mr. Tischler
 Mr. King

Code ME Mr. Hall

Code SV Mr. Nelson

Lewis Research Center:

Mr. Connors
Mr. Conrad
Mr. Dankhoff(3)

Langley Research Center

Mr. Pierpoint
Mr. Corsin